
Enhancing Gradient-based Discrete Sampling via Parallel Tempering

Luxu LIANG¹ Yuhang JIA² Feng ZHOU³

Abstract

While gradient-based discrete samplers are effective in sampling from complex distributions, they are susceptible to getting trapped in local minima, particularly in high-dimensional, multimodal discrete distributions, owing to the discontinuities inherent in these landscapes. To circumvent this issue, we combine parallel tempering, also known as replica exchange, with the discrete Langevin proposal and develop the Parallel Tempering enhanced Discrete Langevin Proposal (PT-DLP), which are simulated at a series of temperatures. Significant energy differences prompt sample swaps, which are governed by a Metropolis criterion specifically designed for discrete sampling to ensure detailed balance is maintained. Additionally, we introduce an automatic scheme to determine the optimal temperature schedule and the number of chains, ensuring adaptability across diverse tasks with minimal tuning. Theoretically, we establish that our algorithm converges non-asymptotically to the target energy and exhibits faster mixing compared to a single chain. Empirical results further emphasize the superiority of our method in sampling from complex, multimodal discrete distributions, including synthetic problems, restricted Boltzmann machines, and deep energy-based models.

1. Introduction

Discrete structures are common in the real world, including statistics (Robert, 1999; Doucet et al., 2000; Ait-Sahalia & Mykland, 2003; Neal, 2000; Ishwaran & James, 2001), physics (Baumgärtner et al., 2012; Zarfaty et al., 2022; Negri et al., 2015), bioinformatics (Bollback, 2006; Yu et al., 2013; Wang et al., 2010), and computer science (Wang & Cho, 2019; Peters & Welling, 2018; Meng et al., 2022; Dawid

& LeCun, 2024), which highlights the need for discrete samplers. Since sampling from a target probability distribution $\pi(\theta) \propto \exp(U(\theta))$ defined on a discrete space Θ is typically intractable, one usually resorts to Markov chain Monte Carlo (MCMC) methods. Recent studies (Zanella, 2020; Grathwohl et al., 2021; Zhang et al., 2022; Sun et al., 2021; 2022; 2023; Xiang et al., 2023; Pynadath et al., 2024) leverage gradient information within discrete distributions to refine proposal distributions, achieving notable advancements in sampling efficiency.

A key limitation of gradient-based methods is their susceptibility to being trapped in local modes due to the reliance on local gradient information (Ziyin et al., 2021; Pynadath et al., 2024), particularly when dealing with well-separated modes, which hinders both accuracy and efficiency in sampling. In continuous domains, various techniques, such as parallel tempering (PT) (Swendsen & Wang, 1986; Chen et al., 2020), cyclical step sizes (Zhang et al., 2019), and flat histograms (Berg & Neuhaus, 1991; Deng et al., 2020c), have been proposed to mitigate this issue. Among these methods, PT is widely used for its ease of implementation and parallelization. By simulating Langevin chains at varying temperatures and incorporating a swap mechanism, PT accelerates convergence while balancing exploration and exploitation. However, in discrete domains, where distributions are inherently more multimodal due to their discontinuous nature, the problem is further exacerbated. Despite the pressing need, limited research has focused on developing gradient-based discrete samplers that can effectively explore multimodal distributions.

In this paper, we introduce the Parallel Tempering enhanced Discrete Langevin Proposal (PTDLP) algorithm, which leverages PT to improve the efficiency and accuracy of gradient-based samplers when sampling from discrete, multimodal distributions. Intuitively, the high-temperature chains act as bridges, facilitating the connection between the various modes. To ensure detailed balance, we employ a tailored Metropolis step to determine swaps. Additionally, with the introduction of multiple chains, we design an automatic scheme to obtain the optimal temperature settings and number of chains for different scenarios. Specifically, we make several contributions:

1) We improve the discrete Langevin proposal (Zhang et al.,

¹School of Mathematics, Renmin University of China

²Department of Mathematical Sciences, Tsinghua University

³Center for Applied Statistics and School of Statistics, Renmin University of China. Correspondence to: Luxu Liang <lianglux@ruc.edu.cn>, Feng Zhou <feng.zhou@ruc.edu.cn>.

2022) for multimodal distributions via PT, optimizing temperature schedules and chain numbers. This method allows easy, customizable adjustments for different datasets with minimal manual input, balancing exploration and exploitation in discrete distributions.

- 2) We provide a non-asymptotic convergence analysis for our method in general discrete distributions, theoretically demonstrating the acceleration effect of multiple chains and explaining the necessity of the Metropolis-Hastings step.
- 3) We demonstrate the superiority of our method for both sampling and learning tasks, including synthetic mixture models, restricted Boltzmann machines, and deep energy-based models.

2. Related Works

2.1. Gradient-based Discrete Sampling

Gradient-based discrete sampling has gained popularity for tackling complex discrete sampling tasks, with its origins rooted in Local Balance Proposals (LBP) (Zanella, 2020), which leverage local density ratios to enhance sampling efficiency. Grathwohl et al. (2021) expanded LBP by incorporating first-order Taylor approximations, ensuring computational feasibility and improving performance. To facilitate sampling in high-dimensional discrete spaces, LBP were further extended to explore larger neighborhoods through a sequence of small moves (Sun et al., 2021). Zhang et al. (2022) proposed Discrete Langevin Proposal (DLP) by adapting continuous Langevin MCMC methods to discrete spaces, allowing parallel updates of all coordinates based on gradient information. Additionally, DLP was refined with an adaptive mechanism to automatically adjust step sizes for better efficiency (Sun et al., 2023). While these approaches have shown promise, challenges persist in sampling from discrete, multimodal distributions.

2.2. Sampling on Multimodal Distributions

Various algorithms have been proposed to enhance exploration in complex, multimodal distributions, including importance sampling (Wang & Landau, 2001), simulated annealing (Kirkpatrick et al., 1983), simulated tempering (Marinari & Parisi, 1992), cyclic step-size scheduling (Zhang et al., 2019), dynamic weighting (Wong & Liang, 1997), and replica exchange Monte Carlo (Swendsen & Wang, 1986; Earl & Deem, 2005). Among these advancements, simulated annealing stochastic gradient Markov chain Monte Carlo (SGMCMC) (Mangoubi & Vishnoi, 2018) and simulated tempering SGMCMC (Ge et al., 2018) show how dynamical temperatures speed up the convergence. However, simulated annealing is very sensitive to the fast-decaying temperatures, and simulated tempering requires a lot on the approximation of the normaliz-

ing constant. The replica exchange Markov chain Monte Carlo (reMCMC) leverages multiple chains operating at different temperatures and allows exchanges between chains, which is easier to implement and suitable for parallelism. Chen et al. (2020) analyzed the acceleration effect of replica exchange in χ^2 divergence and large deviation principle. Dong & Tong (2022) analyzed the mixing properties of reMCMC by evaluating its spectral gap, while Deng et al. (2020a;b) demonstrated its efficiency in large-scale deep learning applications.

Despite the more pronounced multimodal nature of discrete domains due to their inherent discontinuities, research on sampling from multimodal distributions in discrete domains remains limited. Pynadath et al. (2024) proposed a cyclic scheduling strategy that alternates step sizes, enhancing the handling of multimodal distributions. Zheng et al. (2024) attempted to integrate replica exchange with gradient-based sampling; however, their approach lacks a rigorous theoretical foundation, and the two replicas encounter a specific issue, as discussed in Section 4.1.

3. Preliminaries

In this section, we provide a formal definition of the problem and present an overview of the relevant methods.

3.1. Problem Definition

We are concerned with the task of sampling from some target distribution defined over a discrete space $\pi : \Theta \rightarrow [0, 1]$, which is given by

$$\pi(\theta) = \frac{1}{Z} \exp(\beta U(\theta)), \quad \forall \theta \in \Theta, \quad \Theta \subseteq \mathbb{R}^d, \quad (1)$$

where θ is a d -dimensional variable, $\beta = 1$ denotes the inverse temperature parameter, Θ is a finite domain, U represents the energy function, and Z is the normalizing constant. We adopt the following assumptions regarding the domain and the energy function, as commonly found in the literature on gradient-based discrete sampling (Grathwohl et al., 2021; Zhang et al., 2022). Specifically, the sampling domain is factorized coordinate-wise, so that $\Theta = \prod_{i=1}^d \Theta_i$, where we primarily consider binary cases $\Theta = \{0, 1\}^d$ or categorical $\{0, 1, \dots, N\}^d$. The energy function is differentiable¹ across \mathbb{R}^d .

3.2. Replica Exchange Langevin Dynamics

The replica exchange Langevin Dynamics (reLD) is a widely used sampling method for non-convex exploration in continuous spaces. The method updates according to the following

¹Noted that this assumption can be relaxed via Newton’s Series Approximation (Xiang et al., 2023).

dynamics, for $k = 1, \dots, K$ and $i = 1, 2, \dots, I$,

$$\theta_{i+1}^{(k)} = \theta_i^{(k)} + \frac{\alpha_k}{2} \nabla U(\theta_i^{(k)}) + \sqrt{\frac{\alpha_k}{\beta_k}} \xi_k,$$

where $\{\alpha_k\}_{k=1}^K$ represents the step sizes, $\{\beta_k\}_{k=1}^K$ are the inverse temperature parameters, and $\{\xi_k\}_{k=1}^K$ are independent Gaussian noises drawn from $\mathcal{N}(0, I_{d \times d})$. In the typical set-up, the first chain is designated as the low-temperature chain. The gradient $\nabla U(\cdot)$ guides the algorithm toward high-probability regions.

To further improve the mixing rate over Langevin dynamics, reLD enables interaction through a chain-swap mechanism between neighboring replicas. Specifically, the probability to swap the i -th samples between $\theta_i^{(k)}$ and $\theta_i^{(k+1)}$ is determined by $\rho s_k(\theta_i^{(k)}, \theta_i^{(k+1)})$ with $\rho > 0$ being the swapping intensity. The swap function $s_k : \Theta \times \Theta \rightarrow \mathbb{R}^+$ for $k = 1, \dots, K-1$ is given by

$$s_k(\theta_i^{(k)}, \theta_i^{(k+1)}) = \min \left\{ 1, e^{(\beta_k - \beta_{k+1})[U(\theta_i^{(k)}) - U(\theta_i^{(k+1)})]} \right\}.$$

Intuitively, the probability of swap in reLD depends on the energy values in $\theta_i^{(k)}$ and $\theta_i^{(k+1)}$. When the low-temperature chain is trapped in a local minimum and the high-temperature chain explores modes with much lower energy, swapping allows the former to escape and characterize new modes, while the latter continues broader exploration.

3.3. Discrete Langevin Sampler

The Discrete Langevin Proposal (DLP) is a gradient-based approach for sampling from high-dimensional discrete distributions (Zhang et al., 2022). Inspired by Langevin Dynamics, DLP updates all coordinates in parallel using a single gradient computation to function effectively in discrete settings. Specifically, for a target distribution $\pi(\theta) \propto \exp(U(\theta))$, DLP generates a new sample θ' inspired by the Taylor expansion:

$$q(\theta' | \theta) = \frac{\exp\left(-\frac{1}{2\alpha} \|\theta' - \theta - \frac{\alpha}{2} \nabla U(\theta)\|_2^2\right)}{Z_{\Theta}(\theta)},$$

where $\theta, \theta' \in \Theta$, $\nabla U(\theta)$ is the gradient of the energy function evaluated at θ , and $Z_{\Theta}(\theta)$ normalizes the distribution: $Z_{\Theta}(\theta) = \sum_{\theta' \in \Theta} \exp\left(-\frac{1}{2\alpha} \|\theta' - \theta - \frac{\alpha}{2} \nabla U(\theta)\|_2^2\right)$. A key insight is that, for $i = 1, \dots, d$, the update rule can be factorized by coordinate:

$$\text{Cat} \left[\text{Softmax} \left(\frac{1}{2} \nabla U(\theta)_i (\theta'_i - \theta_i) - \frac{1}{2\alpha} (\theta'_i - \theta_i)^2 \right) \right], \quad (2)$$

with $\theta'_i \in \Theta_i$, which makes DLP scalable and computationally efficient for complex distributions. DLP can be implemented with or without the Metropolis-Hastings (MH) step,

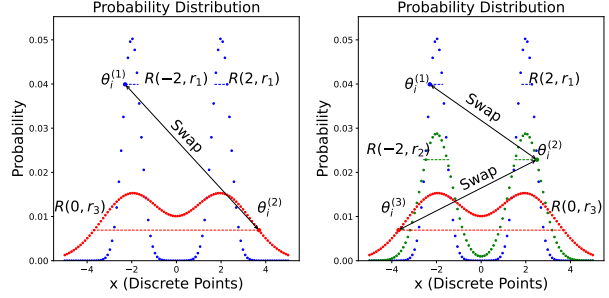


Figure 1. The blue, green, and red dots correspond to probability functions at three temperatures. The high-probability areas to sample from are indicated by dashed lines.

corresponding to the discrete Metropolis adjusted Langevin algorithm (DMALA) and the discrete unadjusted Langevin algorithm (DULA), respectively.

4. Methodology

In this section, we introduce our proposed algorithm in Section 4.1 and discuss the optimal temperature schedule and the number of chains in Sections 4.2 and 4.3.

4.1. Parallel Tempering Enhanced Discrete Langevin Sampler

One major issue with two replicas is that the swaps may not happen often enough. To see this, denote by $R(r, M) := \{x : \|x - r\| \leq M\}$. As shown in Figure 1, the figure on the left illustrates the swap between two chains. The high-probability regions for $\theta_i^{(1)}$ and $\theta_i^{(3)}$ are defined by $R(2, r_1) \cup R(-2, r_1)$ and $R(0, r_3)$. Swaps between $\theta_i^{(1)}$ and $\theta_i^{(3)}$ are unlikely to occur frequently, as $\theta_i^{(3)}$ has a low probability of falling within the region $R(2, r_1) \cup R(-2, r_1)$. However, when the number of chains increases to three, the high-probability region for $\theta_i^{(2)}$ becomes $R(2, r_2) \cup R(-2, r_2)$ with $r_1 < r_2 < r_3$, making it easier for $\theta_i^{(3)}$ to lie within this region, thereby increasing the frequency of swaps. In light of the fact that non-adjacent chain swaps are unlikely to occur, we exclusively consider adjacent swaps in this paper.

Building on the previous discussion, we propose a method that incorporates multiple chains to further enhance performance:

Exploitation:

$$q_1(\theta' | \theta) \propto \exp \left\{ -\frac{\beta_1}{2} \nabla U(\theta)^\top (\theta' - \theta) - \frac{1}{2\alpha_1} \|\theta' - \theta\|_p^p \right\}, \quad (3)$$

Exploration:

$$q_k(\theta' | \theta) \propto \exp \left\{ \underbrace{-\frac{\beta_k}{2} \nabla U(\theta)^\top (\theta' - \theta)}_{\text{First-order Taylor Expansion}} - \underbrace{\frac{1}{2\alpha_k} \|\theta' - \theta\|_p^p}_{\text{Regularizer}} \right\}, \quad (4)$$

where $k = 2, \dots, K$ and $1 = \beta_1 > \dots > \beta_K = 0$. Note that the above proposals can also be factorized by coordinates, as shown in Equation (2), which allows us to update each coordinate in parallel after computing $\nabla U(\theta)$. Zhang et al. (2022) emphasize the importance of the regularizer term, as it introduces a parameter similar to the step size. Note that we have chosen the p -norm instead of the 2-norm, considering that in certain tasks, selecting alternative norms may improve model performance, which could be due to the geometric structure of specific discrete domain distributions (Park et al., 2023; Jiang et al., 2024). We denote the proposal in Equations (3) and (4) by Parallel Tempering enhanced Discrete Langevin Proposal (PTDLP), which needs a MH step (Metropolis et al., 1953). Specifically, for each $k = 1, \dots, K$, after generating the next position θ' from a distribution $q_k(\cdot | \theta)$, the MH step accepts it with the following probability:

$$\min \left\{ 1, \exp(\beta_k (U(\theta') - U(\theta))) \frac{q_k(\theta | \theta')}{q_k(\theta' | \theta)} \right\}. \quad (5)$$

Marginally, $\theta_i^{(k)}$ has its invariant distribution $\pi^{\beta_k}(\theta) \propto \exp(\beta_k U(\theta))$. Unless noted, our algorithm all includes the MH step. The exchange takes place between neighboring replicas. In particular, for each $1 \leq k \leq K - 1$, $\theta_{i+1}^{(k)}$ and $\theta_{i+1}^{(k+1)}$ are swapped with rate ρs_k , where s_k is a tailored Metropolis criterion:

$$s_k \left(\theta_{i+1}^{(k)}, \theta_{i+1}^{(k+1)} \mid \theta_i^{(k)}, \theta_i^{(k+1)} \right) = \max \left\{ 1, e^{\beta_{\delta,k} [U(\theta_{i+1}^{(k)}) + U(\theta_i^{(k)}) - U(\theta_{i+1}^{(k+1)}) - U(\theta_i^{(k+1)})]} \right\}, \quad (6)$$

where $\beta_{\delta,k} := \beta_k - \beta_{k+1}$. This approach involves running multiple chains in parallel, with each chain exploring a unique region of the parameter space. By exchanging information through swaps, the chains can effectively traverse diverse areas of the solution space, reducing the risk of becoming trapped in local minima. This mechanism significantly enhances the algorithm's capacity to effectively explore multimodal distributions. As the number of chains increases, additional parameters, such as the chain number and temperature schedule, must be specified, as discussed in the following sections.

4.2. Optimal Temperature Schedule

Poor spacing of the temperatures can cause the replica systems to be either too far apart, reducing the chances of exchange, or too close, limiting the diversity of the samples (Kone & Kofke, 2005). We are interested in determining the optimal distribution of transition probabilities that maximizes the flow across the inverse temperature space. To this end, we adopt the following assumption, as stated in Syed (2022, Assumption 2).

Algorithm 1 Parallel Tempering Discrete Langevin Proposal (PTDLP for short).

given: Step size α , sampling steps \hat{n} , temperatures \mathcal{T}_K , chain number K , swap intensity ρ , initial samples θ_0 .

loop

for $k = 1, \dots, K$ **do** {Can be done in parallel}

Sampling step

for $i = 1, \dots, d$ **do** {Can be done in parallel}

construct $q_n^{(i)}(\cdot | \theta)$ as in Equation (2)

sample $\theta_n^{(i)} \sim q_n^{(i)}(\cdot | \theta)$

end for

MH step

compute $q(\theta' | \theta) = \prod_i q_i(\theta'_i | \theta)$

and $q(\theta | \theta') = \prod_i q_i(\theta_i | \theta')$

set $\theta \leftarrow \theta'$ with probability in Equation (5)

end for

Swapping step

$u \leftarrow \text{Unif}(0, 1)$

for $k = 1, \dots, K - 1$ **do**

construct s_n as in Equation (6)

$\hat{s}_n \leftarrow \hat{s}_n + s_n$

exchange θ_k and θ_{k+1} if $u \leq \rho s_n$

end for

end loop

$\hat{s}_k \leftarrow \hat{s}_k / \hat{n}$ for all $k \in \{1, \dots, K - 1\}$

output: Samples $\{\theta_1(t)\}_{t=1}^{\hat{n}}$ and acceptance rates $\{\hat{s}_k\}_{k=1}^{K-1}$.

Assumption 4.1. For any $k = 1, \dots, K$ and $\theta \sim \pi^{\beta_k}$ and $\theta' \sim q_k(\theta' | \theta)$, the r.v. $U(\theta)$ and $U(\theta')$ are independent.

Note that Assumption 4.1 is not expected to hold exactly in real scenarios. Syed (2022) has shown that even when Assumption 4.1 is violated, the key results made by the theory still closely match empirical behavior. Furthermore, this simplifying assumption on the local exploration moves allows us to decouple the sampler and specifically analyze the impact of temperature selection on the efficiency of PT. In PT literature, τ is commonly referred to as the round trip rate and has been used to compare the effectiveness of various PT algorithms (Katzgraber et al., 2006; Lingenheil et al., 2009). In the next theorem, we calculate the round trip rate of the algorithm we propose.

Theorem 4.2. Let Assumption 4.1 hold. For any fixed chain number K and temperature schedule $\mathcal{T}_K = \{\beta_1, \dots, \beta_K\}$, the non-asymptotic (in K) round trip rate of PT with all neighboring chains swapping is

$$\tau(\mathcal{T}_K) = \frac{K}{(K+1) \sum_{k=1}^{K-1} (1/s_k)},$$

where s_k , defined in Equation (6), is the probability of swapping between chains k and $k+1$.

We first discuss how to optimize the temperature schedule \mathcal{T}_K to maximize the round trip rate $\tau(\mathcal{T}_K)$ when K is fixed. Let $\tilde{s}(\beta_k, \beta_{k+1}) := s_k$, where s_k is defined in Equation (6), and define $\lambda(\beta) := \lim_{\delta \rightarrow 0} \frac{1 - \tilde{s}(\beta, \beta + \delta)}{|\delta|}$. The communication barrier is expressed as the integral of λ , given by $\Lambda(\beta) = \int_0^\beta \lambda(t) dt$, with Λ denoting $\Lambda(1)$ and $\Lambda(0) = 0$. By using Syed (2022, Corollary 2), we obtain $\sum_{k=1}^{K-1} (1 - s_k) \approx \Lambda$ for all temperature schedules. Therefore, our task becomes to maximize $\tau(\mathcal{T}_K)$, subject to the constraint $\sum_{k=1}^{K-1} (1 - s_k) = \Lambda$ and $0 \leq s_k \leq 1$, which implies that the non-asymptotic round trip rate is maximized when the swap rates are all equal². Then we get

$$\Lambda(\beta_k^*) / \Lambda \approx 1 - \frac{k-1}{K-1}. \quad (7)$$

To obtain the estimation of the communication barrier Λ , we first perform a short pilot run and have access to a collection of samples $(\tilde{\theta}_1, \tilde{\theta}_2, \dots, \tilde{\theta}_{\tilde{n}})$ with $\tilde{\theta}_i := (\tilde{\theta}_i^{(1)}, \dots, \tilde{\theta}_i^{(K)})^\top$ from our algorithm based on an arbitrary temperature schedule \mathcal{T}_K . For the given schedule \mathcal{T}_K , the Monte Carlo estimates for the acceptance rates satisfy

$$\hat{s}_k \approx \frac{1}{\tilde{n}-1} \sum_{i=1}^{\tilde{n}-1} s_k \left(\tilde{\theta}_{i+1}^{(k)}, \tilde{\theta}_{i+1}^{(k+1)} \mid \tilde{\theta}_i^{(k)}, \tilde{\theta}_i^{(k+1)} \right).$$

Equation (7) motivates the following approximation for $\Lambda(\beta_k)$, for $k = 1, \dots, K-1$,

$$\hat{\Lambda}(\beta_k) = \sum_{i=k}^{K-1} (1 - \hat{s}_i). \quad (8)$$

Given $\hat{\Lambda}(\beta_1), \dots, \hat{\Lambda}(\beta_K)$, we estimate the function $\Lambda(\beta)$ via a monotone piecewise cubic interpolation (Fritsch & Carlson, 1980). The optimal temperature schedule can be determined using the bisection method based on Equation (7).

4.3. Optimal Chain Number

Fixing the temperature schedule, we now aim to improve the algorithm by modifying the number of chains. Suppose there are \mathcal{B} copies of PT running in parallel, each consisting of K chains with their optimal temperature schedules. If \bar{K} represents the total number of available machines, then K must satisfy the constraint $\mathcal{B}K \leq \bar{K}$. The total round trip rate across all \mathcal{B} copies of PT is

$$\tau_\Lambda(K) = \mathcal{B}\tau(\mathcal{T}_K) = \frac{\mathcal{B}K}{(K+1) \sum_{k=1}^{K-1} \frac{1}{s_k}}.$$

The next proposition explains how to determine the optimal number of chains, given the optimal temperature schedule.

²This result of the identical acceptance rate is highly consistent with the predictions of other existing theoretical frameworks (Atchadé et al., 2011; Predescu et al., 2004; Syed, 2022).

Proposition 4.3. $\tau_\Lambda(\cdot)$ is optimized when we run $\mathcal{B}^* = \bar{K} / K^*$ copies of PT with $K^* = \frac{2+3\Lambda+\sqrt{9\Lambda^2+20\Lambda+4}}{4}$ chains to achieve an optimum round trip rate.

Details of the iterative schedule tuning algorithm can be found in Appendix B.

5. Theoretical Analysis

In this section, we present an asymptotic convergence analysis of PTDL without MH step, along with its mixing time, and a non-asymptotic convergence analysis for PTDL with MH step, which extends the previous analysis (Grathwohl et al., 2021; Zhang et al., 2022; Pynadath et al., 2024). We further highlight the acceleration benefits achieved through swapping mechanism.

5.1. Asymptotic Convergence Analysis

First, we prove the asymptotic convergence of PTDL without MH. Zhang et al. (2022) showed that a discrete Langevin-like sampler with temperature 1 is reversible for log-quadratic energy distributions with small step sizes. However, this does not directly extend to the proposed algorithm due to the multi-chain structure, swap mechanism, and higher temperatures. We focus on the case of three chains, with the result extendable to more.

Theorem 5.1. Let $\pi^{\beta_1} \propto \exp(\beta_1 U(\theta))$ be the target distribution and $\tilde{\pi}^{\beta_1}(\theta) \propto \exp(\beta_1(\theta^\top W\theta + b\theta))$ be the log-quadratic distribution satisfying that $\exists W \in \mathbb{R}^{d \times d}$, $b \in \mathbb{R}$, $\epsilon \in \mathbb{R}^+$, such that $\|\nabla U(\theta) - (2W\theta + b)\|_1 \leq \epsilon$ for any $\theta \in \Theta$, then the stationary distribution of PTDL without MH satisfies

$$\|\pi_\alpha - \pi\|_1 \leq Z_1 (\exp(Z_2\epsilon) - 1) + Z_3 \exp\left(-\frac{1 + \alpha\beta_1\lambda_{\min}}{2\alpha}\right), \quad (9)$$

where λ_{\min} is the smallest eigenvalue of W , Z_1 is a constant determined by $\tilde{\pi}^{\beta_1}$ and α , Z_2 denotes a constant influenced by Θ and $\max_{\theta, \theta' \in \Theta} \|\theta' - \theta\|_\infty$, while Z_3 corresponds to a constant that is dependent on $\tilde{\pi}^{\beta_1}$.

The first term represents the bias due to π deviating from log-quadratic, while the second term reflects the bias from using a non-zero step size. However, as shown in the following theorem, reducing the step size to mitigate the second-term error is impractical in real-world applications.

Theorem 5.2. If the target distribution is assumed to be log-quadratic, i.e., for any $\theta \in \Theta$, $\pi(\theta) \propto \exp\{\theta^\top W\theta + b^\top \theta\}$ with some constants $W \in \mathbb{R}^{d \times d}$ and $b \in \mathbb{R}^d$. Denote by $\mathcal{D} = \sup_{\theta, \theta' \in \Theta} \|\theta - \theta'\|$. The mixing time of PTDL

without MH step defined in Equation (20) satisfies

$$t_{\text{mix}}(\varepsilon) \geq \left(\frac{1}{4Z} \exp \left(\frac{1}{2} \lambda_{\min}(W) \mathcal{D}^2 + \frac{1}{2\alpha} \mathcal{D}^p \right) - 1 \right) \log \left(\frac{1}{2\varepsilon} \right).$$

Without the MH step, the error between our algorithm's stationary distribution and the target distribution arises from two sources: the distance to the log-quadratic distribution (quantified by the first term in Equation (9)) and the error introduced by the step size. Zhang et al. (2022) noted that for small step sizes, this error can be neglected, and removing the MH step reduces computational costs. However, Theorem 5.2 shows that as the step size decreases, mixing time increases exponentially, adding computational costs. Furthermore, in discrete domains, the decaying step sizes used in continuous settings are not applicable. To ensure convergence with fixed step sizes, the MH step is required.

5.2. Non-asymptotic Convergence Analysis

Next, we focus on proving the non-asymptotic convergence of PTDLP with MH. We have the following assumptions:

Assumption 5.3. The function $U(\cdot) \in C^2(\mathbb{R}^d)$ has M -Lipschitz gradient. That is

$$\|\nabla U(\theta) - \nabla U(\theta')\| \leq M \|\theta - \theta'\|.$$

Assumption 5.4. For each $\theta \in \Theta$, there exists an open ball containing θ of some radius r_θ , denoted by $R(\theta, r_\theta)$, such that the function $U(\cdot)$ is m -strongly concave in $R(\theta, r_\theta)$ for some $m > 0$.

Assumptions 5.3 and 5.4 are standard in optimization and sampling literature (Dalalyan, 2017). For simplicity of the proof, we consider the case of three chains. Denote by

$$\tilde{\mathcal{D}}(\Theta) := \max \left\{ \sup_{\theta, \theta' \in \Theta} \|\theta - \theta'\|, \sqrt{\frac{2 \log(1/\varepsilon_0)}{\|\mathcal{T}_K\| (M - \frac{m}{2})}} \right\}, \quad (10)$$

where $0 < \varepsilon_0 < 1$ is given by Equation (34) and $\|\mathcal{T}_K\| := \min_{k=1, \dots, K-1} |\beta_k - \beta_{k+1}|$.

Theorem 5.5. Let Assumptions 5.3 and 5.4 hold. Then for the Markov chain P with three chains, we have, for any $\theta', \theta^{(1)}$, and $\theta^{(2)} \in \Theta$,

$$p(\theta' | \theta_i^{(1)}) \geq \varepsilon \frac{\exp\{\beta_3 U(\theta')\}}{\sum_{\theta' \in \Theta} \exp\{\beta_3 U(\theta')\}},$$

where $\varepsilon = \varepsilon_0^2 \varepsilon_{\beta_3, \alpha}$ with ε_0 given in Equation (34) and

$$\varepsilon_{\beta_3, \alpha} = \exp \left\{ - \left(\beta_3 M - \frac{\beta_3 m}{2} \right) \tilde{\mathcal{D}}(\Theta)^2 - \beta_3 \|\nabla U(a)\| \tilde{\mathcal{D}}(\Theta) - \frac{1}{\alpha} \tilde{\mathcal{D}}(\Theta)^p \right\},$$

with $a \in \arg \min_{\theta \in \Theta} \|\nabla U(\theta)\|$.

Corollary 5.6. Let Assumptions 5.3 and 5.4 hold. Then for the Markov chain P with three chains, the following hold:

1) P is uniformly ergodic with

$$\|P^n - \pi\|_{TV} \leq (1 - \varepsilon)^n.$$

2) For any real-valued function f and samples $\theta_1, \dots, \theta_n$ from P , one has

$$\sqrt{n} \left(\frac{1}{n} \sum_{i=1}^n f(X_i) - \sum_{\theta \in \Theta} f(\theta) \pi(\theta) \right) \xrightarrow{d} N(0, \tilde{\sigma}_*^2),$$

for some $\tilde{\sigma}_* > 0$ as $n \rightarrow \infty$.

The proof follows directly from Theorem 5.5 and Jones (2004) [Corollary 5]. Corollary 5.6 shows that swapping increases ε , leading to a faster convergence rate to the invariant distribution. Thus, we have the following corollary.

Corollary 5.7. Let Assumptions 5.3 and 5.4 hold. Assume that

$$\|\nabla U(a)\| < (M - \frac{m}{2}) \tilde{\mathcal{D}}(\Theta) - \frac{2 \log(1/\varepsilon_0)}{\|\mathcal{T}_K\| \tilde{\mathcal{D}}(\Theta)},$$

where $a \in \arg \min_{\theta \in \Theta} \|\nabla U(\theta)\|$ and $\tilde{\mathcal{D}}(\Theta)$ is in Equation (10). Then, our algorithm converges faster than DLP.

6. Experiments

In this section, we evaluate the newly proposed method on four problem types: (1) sampling from synthetic distributions, (2) sampling from restricted Boltzmann machines on real-world datasets, (3) learning restricted Boltzmann machines and (4) deep energy-based models parameterized by a convolutional neural network.

For sampling tasks, we compare our algorithm with several popular gradient-based discrete samplers: the discrete Langevin-like samplers (DULA and DMALA) (Zhang et al., 2022), the any-scale balanced sampler (AB) (Sun et al., 2023), and the automatic cyclical sampler (ACS) (Pynadath et al., 2024). For learning tasks, we exclude the AB sampler, as it is not originally designed for model learning applications. More details such as experimental setups, hyper-parameters, and additional experimental results can refer to Appendix F. We released the code of the synthetic task at <https://github.com/LuxLiang/PTDLP/tree/main>.

6.1. Synthetic Problems

We first address the challenges of sampling from two-dimensional discrete multimodal distributions, specifically mixtures of Gaussian components (MoG) and mixtures of Student's t-distributions (MoS), defined over the domain $\Theta = \{1, 2, \dots, 101\}^2$. To quantify the ability to

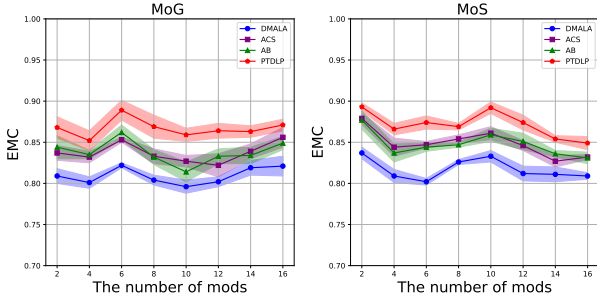


Figure 2. Sampling performance (measured by EMC) of various methods for Mixture of Gaussian (left) and Mixture of Student’s t-distributions (right) with varying components. PTDLP consistently outperforms baselines across random seeds.

Table 1. Experiment results with exploring MoG and MoS, measured by KL and MMD (c denotes the number of components).

Metrics / Samplers	MoG (c=8)	MoG (c=16)	MoS (c=8)	MoS (c=16)	
MMD (\downarrow)	DMALA	2.077 \pm 0.022	2.030 \pm 0.012	2.017 \pm 0.021	2.158 \pm 0.023
	ACS	2.004 \pm 0.011	2.006 \pm 0.013	2.006 \pm 0.017	2.013 \pm 0.021
	AB	2.019 \pm 0.036	2.001 \pm 0.012	2.005 \pm 0.024	2.015 \pm 0.018
	PTDLP	1.996 \pm 0.025	1.924 \pm 0.011	1.934 \pm 0.038	1.967 \pm 0.015
KL (10^{-2}) (\downarrow)	DMALA	1.331 \pm 0.032	7.660 \pm 0.043	2.017 \pm 0.026	7.674 \pm 0.029
	ACS	0.662 \pm 0.012	2.177 \pm 0.023	3.117 \pm 0.041	3.112 \pm 0.017
	AB	0.851 \pm 0.011	3.216 \pm 0.022	2.801 \pm 0.026	2.871 \pm 0.021
	PTDLP	0.617 \pm 0.009	2.133 \pm 0.017	0.667 \pm 0.017	1.948 \pm 0.014

avoid mode collapse, we use Maximum Mean Discrepancy (MMD) (Gretton et al., 2012), forward Kullback-Leibler divergence (Kullback & Leibler, 1951), and Entropic Mode Coverage (EMC) (Blessing et al., 2024) as quantitative performance metrics. $\text{EMC} \in [0, 1]$ is a heuristic metric for mode collapse detection, where 0 indicates samples come from a single mode, and 1 indicates samples cover all modes.

Results As shown in Table 1 and Figure 2, the PTDLP algorithm consistently outperforms other methods on both mixed Gaussian and t-distributions with varying components across different metrics. While methods like AB and ACS attempt to alleviate this issue through variable step sizes, their effectiveness still falls short compared to our approach. These results underscore the algorithm’s exceptional performance in these synthetic problems, while effectively mitigating mode collapse.

Analysis The superior performance of our algorithm arises from simultaneously simulating multiple chains at different temperatures. As the number of modes in synthetic distributions increases or the modes become well-separated, a single chain often fails to effectively explore the global distribution, becoming vulnerable to local minima. Using multiple chains, however, allows for a more thorough exploration of the different modes, enhancing coverage of the entire distribution and mitigating the risk of getting trapped in local minima.

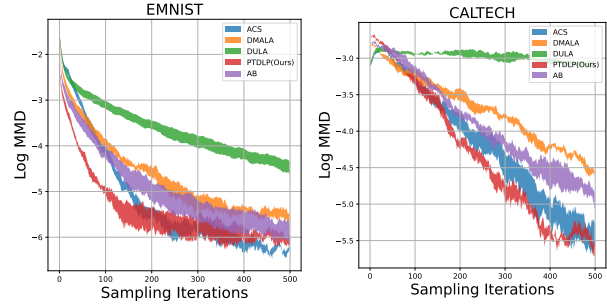


Figure 3. RBM sampling results with mode initialization. PTDLP achieves faster convergence, while baseline methods converge slower due to being trapped in the mode.

6.2. Sampling From Restricted Boltzmann Machines

Restricted Boltzmann Machines (RBMs) are generative artificial neural networks, which learn an unnormalized probability over inputs:

$$U(\theta) = \sum_i \text{Softplus}(W\theta + a)_i + b^\top \theta,$$

where $\{W, a, b\}$ are parameters and $\theta \in \{0, 1\}^d$. Following Grathwohl et al. (2021) and Zhang et al. (2022), we train $\{W, a, b\}$ with contrastive divergence (Carreira-Perpinan & Hinton, 2005) on various datasets for one epoch. We measure the MMD between the obtained samples and those from block-Gibbs sampling, which utilizes the known structure and can be regarded as the ground truth. To further test whether our method can escape local modes, we initialize all samplers to start within the most likely mode of the dataset as measured by the model distribution.

Results As shown in Table 2, our algorithm consistently demonstrates superior performance across a diverse array of complex real-world datasets, with notable improvements in datasets like Caltech. AB and ACS perform nearly as well but with slightly higher MMD values. In Figure 3, our approach converges more quickly than other samplers, yielding competitive results across different random seeds. In contrast, the DULA algorithm with an optimal step size easily becomes trapped in a single mode. These results suggest that our method effectively avoids getting trapped in the initial mode, a challenge faced by the baseline methods.

Analysis These results underscore PTDLP’s ability to efficiently explore and accurately capture multiple modes. In RBM sampling task, the energy landscapes contain many local minima, making it difficult for baseline sampling methods to explore the entire distribution effectively. Our algorithm addresses this and provides the most robust sampling by running multiple chains at different temperatures, allowing higher-temperature chains to explore the space more freely and avoid getting stuck in local minima.

Table 2. RBM sampling results with random initialization and RBM learning results. The top table shows results quantified by *log-MMD* (\downarrow), where PTDL P outperforms all gradient-based baselines across datasets. The bottom table presents *log-likelihood scores* (\uparrow) for RBM learning on test data, as estimated by AIS. PTDL P demonstrates competitive, and sometimes superior, performance across all datasets.

Dataset		DULA	DMALA	AB	ACS	PTDL P (<i>Ours</i>)
RBM Sampling (<i>log-MMD</i> \downarrow)	MNIST	-4.77 \pm 0.34	-6.45 \pm 0.29	-6.65 \pm 0.10	-6.66 \pm 0.20	-6.68\pm0.19
	eMNIST	-3.19 \pm 0.07	-3.85 \pm 0.10	-4.01 \pm 0.12	-3.97 \pm 0.09	-4.05\pm0.09
	kMNIST	-4.03 \pm 0.10	-4.62 \pm 0.17	-4.71 \pm 0.11	-4.58 \pm 0.12	-4.77\pm0.20
	Omniglot	-6.45 \pm 0.15	-6.48 \pm 0.08	-6.48 \pm 0.11	-6.49 \pm 0.18	-6.56\pm0.05
	Caltech	-3.09 \pm 0.10	-4.10 \pm 0.28	-4.21 \pm 0.33	-4.21 \pm 0.20	-4.98\pm0.23
Learning RBM (<i>log-likelihood</i> \uparrow)	MNIST	-386.21 \pm 2.32	-264.83 \pm 1.51	—	-231.12 \pm 2.10	-225.56\pm2.25
	eMNIST	-337.27 \pm 4.21	-324.34 \pm 2.13	—	-301.42\pm1.99	-302.78 \pm 1.95
	kMNIST	-502.22 \pm 3.76	-436.35 \pm 2.76	—	-407.39 \pm 3.46	-362.85\pm3.97
	Omniglot	-228.23 \pm 2.12	-222.61 \pm 1.33	—	-220.71 \pm 1.65	-179.54\pm2.01
	Caltech	-452.97 \pm 6.10	-427.29 \pm 3.99	—	-380.67 \pm 3.01	-346.65\pm2.76

6.3. Learning Energy Based Models

Energy-based models (EBMs) have achieved notable success in machine learning (LeCun et al., 2006; Ngiam et al., 2011). In EBMs, the probability of a data point x is given by $P_\theta(x) = \exp[E_\theta(x)]/Z_\theta$, where $E_\theta(x)$ is the energy function and $Z_\theta = \mathbb{E}_{\theta \sim \Theta}[\exp[E_\theta(x)]]$ is the partition function. MCMC methods are widely used for training EBMs, enabling efficient sampling.

6.3.1. LEARNING RBM

We begin with learning RBM, use the same RBM structure as the sampling task, and apply the samplers of interest to the PCD algorithm introduced by Tieleman (2008). To evaluate the learned model, we employ Annealed Importance Sampling (AIS) (Neal, 2001) with Block-Gibbs to calculate the log-likelihood values. We run AIS for 100,000 steps, which is adequate given the efficiency of Block Gibbs for this specific model.

Results In Table 2, we find that our algorithm produces competitive results compared to the baselines, and in many cases outperforms them across all datasets, demonstrating the superiority and robustness of using multiple chains.

6.3.2. LEARNING DEEP EBM

We train deep EBMs using a ResNet (He et al., 2016) with Persistent Contrastive Divergence (PCD) (Tieleman & Hinton, 2009) and a replay buffer (Du & Mordatch, 2019) on the MNIST, Omniglot, and Caltech datasets, following the approach outlined by Grathwohl et al. (2021); Zhang et al. (2022). We use 10 sample steps per iteration on all datasets except Caltech, where we use 30. After training, we use AIS to estimate the likelihood.

Results The results in Table 3 show that our method is capable of learning better quality EBMs than DMALA and ACS, which can be attributed to the fact that our method

Table 3. Deep Convolution EBM *log likelihood scores* (\uparrow) on test data as estimated by AIS.

	DMALA	ACS	PTDL P (<i>Ours</i>)
Static MNIST	-80.031 \pm 0.038	-79.905 \pm 0.057	-79.622\pm0.063
Dynamic MNIST	-80.120 \pm 0.036	-79.634 \pm 0.024	-79.463\pm0.076
Omniglot	-99.243 \pm 2.101	-91.487 \pm 0.128	-90.976\pm0.316
Caltech	-98.001 \pm 0.371	-89.262 \pm 0.290	-87.192\pm0.343

employs different temperatures to simultaneously explore diverse regions, enabling the identification of more modes.

Analysis In learning tasks, data typically comes from complex, high-dimensional distributions. Our approach runs multiple chains in parallel, where high-temperature chains provide greater exploration capabilities and low-temperature chains focus on more precisely exploiting the existing mode. This strategy effectively overcomes the problem of local minima, allowing the model to navigate the energy barriers between multiple modes, resulting in better solutions for complex distributions. Furthermore, the outstanding results also demonstrate the proposed swap mechanism in Equation (6) effectively corrects imbalance, which leads to improved log-likelihood estimates across diverse image datasets.

7. Conclusions

In this paper, we propose the *Parallel Tempering enhanced Discrete Langevin Proposal* algorithm to better capture multimodal distributions in discrete spaces. Gradient-based samplers are prone to getting trapped in local modes, hindering full exploration of target distributions. To address this, we incorporate parallel tempering for more effective mode exploration. We also optimize the extra hyperparameters, such as the temperature schedule and the number of chains, by maximizing the round trip rate. Additionally, we establish the non-asymptotic convergence bound and

provide extensive experimental results.

Limitations and future work: While we have developed a reversible algorithm with a non-asymptotic result, Syed (2022); Deng et al. (2023) showed that non-reversible parallel tempering often outperforms the reversible version. Future work could explore combining non-reversible methods with discrete samplers. Another limitation is the tailored Metropolis criterion, which may fail in mini-batch settings. Approaches from the continuous domain (Seita et al., 2016; Deng et al., 2020a) could be applied in future research.

Impact Statement

This paper presents work whose goal is to advance the field of Machine Learning. There are many potential societal consequences of our work, none which we feel must be specifically highlighted here.

References

- Ait-Sahalia, Y. and Mykland, P. A. The effects of random and discrete sampling when estimating continuous-time diffusions. *Econometrica*, 71(2):483–549, 2003.
- Atchadé, Y. F., Roberts, G. O., and Rosenthal, J. S. Towards optimal scaling of metropolis-coupled markov chain monte carlo. *Statistics and Computing*, 21:555–568, 2011.
- Baumgärtner, A., Burkitt, A., Ceperley, D., De Raedt, H., Ferrenberg, A., Heermann, D., Herrmann, H., Landau, D., Levesque, D., von der Linden, W., et al. *The Monte Carlo method in condensed matter physics*, volume 71. Springer Science & Business Media, 2012.
- Berg, B. A. and Neuhaus, T. Multicanonical algorithms for first order phase transitions. *Physics Letters B*, 267(2): 249–253, 1991.
- Blessing, D., Jia, X., Esslinger, J., Vargas, F., and Neumann, G. Beyond elbos: A large-scale evaluation of variational methods for sampling. *arXiv preprint arXiv:2406.07423*, 2024.
- Bollback, J. P. Simmap: stochastic character mapping of discrete traits on phylogenies. *BMC bioinformatics*, 7: 1–7, 2006.
- Carreira-Perpinan, M. A. and Hinton, G. On contrastive divergence learning. In *International workshop on artificial intelligence and statistics*, pp. 33–40. PMLR, 2005.
- Chen, Y., Chen, J., Dong, J., Peng, J., and Wang, Z. Accelerating nonconvex learning via replica exchange langevin diffusion. *arXiv preprint arXiv:2007.01990*, 2020.
- Dalalyan, A. S. Theoretical guarantees for approximate sampling from smooth and log-concave densities. *Journal of the Royal Statistical Society Series B: Statistical Methodology*, 79(3):651–676, 2017.
- Dawid, A. and LeCun, Y. Introduction to latent variable energy-based models: a path toward autonomous machine intelligence. *Journal of Statistical Mechanics: Theory and Experiment*, 2024(10):104011, 2024.
- Deng, W., Feng, Q., Gao, L., Liang, F., and Lin, G. Non-convex learning via replica exchange stochastic gradient mcmc. In *International Conference on Machine Learning*, pp. 2474–2483. PMLR, 2020a.
- Deng, W., Feng, Q., Karagiannis, G., Lin, G., and Liang, F. Accelerating convergence of replica exchange stochastic gradient mcmc via variance reduction. *arXiv preprint arXiv:2010.01084*, 2020b.
- Deng, W., Lin, G., and Liang, F. A contour stochastic gradient langevin dynamics algorithm for simulations of multi-modal distributions. *Advances in neural information processing systems*, 33:15725–15736, 2020c.
- Deng, W., Zhang, Q., Feng, Q., Liang, F., and Lin, G. Non-reversible parallel tempering for deep posterior approximation. In *Proceedings of the AAAI Conference on Artificial Intelligence*, volume 37, pp. 7332–7339, 2023.
- Dong, J. and Tong, X. T. Spectral gap of replica exchange langevin diffusion on mixture distributions. *Stochastic Processes and their Applications*, 151:451–489, 2022.
- Doucet, A., Godsill, S., and Andrieu, C. On sequential monte carlo sampling methods for bayesian filtering. *Statistics and computing*, 10:197–208, 2000.
- Du, Y. and Mordatch, I. Implicit generation and modeling with energy based models. *Advances in Neural Information Processing Systems*, 32, 2019.
- Earl, D. J. and Deem, M. W. Parallel tempering: Theory, applications, and new perspectives. *Physical Chemistry Chemical Physics*, 7(23):3910–3916, 2005.
- Fritsch, F. N. and Carlson, R. E. Monotone piecewise cubic interpolation. *SIAM Journal on Numerical Analysis*, 17(2):238–246, 1980.
- Ge, R., Lee, H., and Risteski, A. Simulated tempering langevin monte carlo ii: An improved proof using soft markov chain decomposition. *arXiv preprint arXiv:1812.00793*, 2018.
- Grathwohl, W., Swersky, K., Hashemi, M., Duvenaud, D., and Maddison, C. Oops i took a gradient: Scalable sampling for discrete distributions. In *International Conference on Machine Learning*, pp. 3831–3841. PMLR, 2021.

- Gretton, A., Borgwardt, K. M., Rasch, M. J., Schölkopf, B., and Smola, A. A kernel two-sample test. *The Journal of Machine Learning Research*, 13(1):723–773, 2012.
- He, K., Zhang, X., Ren, S., and Sun, J. Deep residual learning for image recognition. In *Proceedings of the IEEE conference on computer vision and pattern recognition*, pp. 770–778, 2016.
- Horn, R. A. and Johnson, C. R. *Matrix analysis*. Cambridge university press, 2012.
- Ishwaran, H. and James, L. F. Gibbs sampling methods for stick-breaking priors. *Journal of the American statistical Association*, 96(453):161–173, 2001.
- Jiang, Y., Aragam, B., and Veitch, V. Uncovering meanings of embeddings via partial orthogonality. *Advances in Neural Information Processing Systems*, 36, 2024.
- Jones, G. L. On the markov chain central limit theorem. *Probability Surveys*, 1:299–320, 2004.
- Katzgraber, H. G., Trebst, S., Huse, D. A., and Troyer, M. Feedback-optimized parallel tempering monte carlo. *Journal of Statistical Mechanics: Theory and Experiment*, 2006(03):P03018, 2006.
- Kingma, D. P. Adam: A method for stochastic optimization. *arXiv preprint arXiv:1412.6980*, 2014.
- Kirkpatrick, S., Gelatt Jr, C. D., and Vecchi, M. P. Optimization by simulated annealing. *science*, 220(4598):671–680, 1983.
- Kone, A. and Kofke, D. A. Selection of temperature intervals for parallel-tempering simulations. *The Journal of chemical physics*, 122(20), 2005.
- Kullback, S. and Leibler, R. A. On information and sufficiency. *The annals of mathematical statistics*, 22(1):79–86, 1951.
- LeCun, Y., Chopra, S., Hadsell, R., Ranzato, M., Huang, F., et al. A tutorial on energy-based learning. *Predicting structured data*, 1(0), 2006.
- Levin, D. A. and Peres, Y. *Markov chains and mixing times*, volume 107. American Mathematical Soc., 2017.
- Lingenheil, M., Denschlag, R., Mathias, G., and Tavan, P. Efficiency of exchange schemes in replica exchange. *Chemical Physics Letters*, 478(1-3):80–84, 2009.
- Mangoubi, O. and Vishnoi, N. K. Convex optimization with unbounded nonconvex oracles using simulated annealing. In *Conference On Learning Theory*, pp. 1086–1124. PMLR, 2018.
- Marinari, E. and Parisi, G. Simulated tempering: a new monte carlo scheme. *Europhysics letters*, 19(6):451, 1992.
- Meng, C., Choi, K., Song, J., and Ermon, S. Concrete score matching: Generalized score matching for discrete data. *Advances in Neural Information Processing Systems*, 35:34532–34545, 2022.
- Metropolis, N., Rosenbluth, A. W., Rosenbluth, M. N., Teller, A. H., and Teller, E. Equation of state calculations by fast computing machines. *The journal of chemical physics*, 21(6):1087–1092, 1953.
- Neal, R. M. Markov chain sampling methods for dirichlet process mixture models. *Journal of computational and graphical statistics*, 9(2):249–265, 2000.
- Neal, R. M. Annealed importance sampling. *Statistics and computing*, 11:125–139, 2001.
- Negri, F., Manzoni, A., and Amsallem, D. Efficient model reduction of parametrized systems by matrix discrete empirical interpolation. *Journal of Computational Physics*, 303:431–454, 2015.
- Ngiam, J., Chen, Z., Koh, P. W., and Ng, A. Y. Learning deep energy models. In *Proceedings of the 28th international conference on machine learning (ICML-11)*, pp. 1105–1112, 2011.
- Park, K., Choe, Y. J., and Veitch, V. The linear representation hypothesis and the geometry of large language models. *arXiv preprint arXiv:2311.03658*, 2023.
- Peters, J. W. and Welling, M. Probabilistic binary neural networks. *arXiv preprint arXiv:1809.03368*, 2018.
- Predescu, C., Predescu, M., and Ciobanu, C. V. The incomplete beta function law for parallel tempering sampling of classical canonical systems. *The Journal of chemical physics*, 120(9):4119–4128, 2004.
- Pynadath, P., Bhattacharya, R., Hariharan, A., and Zhang, R. Gradient-based discrete sampling with automatic cyclical scheduling. *arXiv preprint arXiv:2402.17699*, 2024.
- Ramachandran, P., Zoph, B., and Le, Q. V. Searching for activation functions. *arXiv preprint arXiv:1710.05941*, 2017.
- Robert, C. Monte carlo statistical methods, 1999.
- Schweitzer, P. J. Perturbation theory and finite markov chains. *Journal of Applied Probability*, 5(2):401–413, 1968.
- Seita, D., Pan, X., Chen, H., and Canny, J. An efficient minibatch acceptance test for metropolis-hastings. *arXiv preprint arXiv:1610.06848*, 2016.

- Sun, H., Dai, H., Xia, W., and Ramamurthy, A. Path auxiliary proposal for mcmc in discrete space. In *International Conference on Learning Representations*, 2021.
- Sun, H., Dai, H., and Schuurmans, D. Optimal scaling for locally balanced proposals in discrete spaces. *Advances in Neural Information Processing Systems*, 35:23867–23880, 2022.
- Sun, H., Dai, B., Sutton, C., Schuurmans, D., and Dai, H. Any-scale balanced samplers for discrete space. In *The Eleventh International Conference on Learning Representations*, 2023.
- Swendsen, R. H. and Wang, J.-S. Replica monte carlo simulation of spin-glasses. *Physical review letters*, 57(21):2607, 1986.
- Syed, S. *Non-reversible parallel tempering on optimized paths*. PhD thesis, University of British Columbia, 2022.
- Tieleman, T. Training restricted boltzmann machines using approximations to the likelihood gradient. In *Proceedings of the 25th international conference on Machine learning*, pp. 1064–1071, 2008.
- Tieleman, T. and Hinton, G. Using fast weights to improve persistent contrastive divergence. In *Proceedings of the 26th annual international conference on machine learning*, pp. 1033–1040, 2009.
- Wang, A. and Cho, K. Bert has a mouth, and it must speak: Bert as a markov random field language model. *arXiv preprint arXiv:1902.04094*, 2019.
- Wang, F. and Landau, D. P. Efficient, multiple-range random walk algorithm to calculate the density of states. *Physical review letters*, 86(10):2050, 2001.
- Wang, J., Huda, A., Lunyak, V. V., and Jordan, I. K. A gibbs sampling strategy applied to the mapping of ambiguous short-sequence tags. *Bioinformatics*, 26(20):2501–2508, 2010.
- Wong, W. H. and Liang, F. Dynamic weighting in monte carlo and optimization. *Proceedings of the National Academy of Sciences*, 94(26):14220–14224, 1997.
- Xiang, Y., Zhu, D., Lei, B., Xu, D., and Zhang, R. Efficient informed proposals for discrete distributions via newton’s series approximation. In *International Conference on Artificial Intelligence and Statistics*, pp. 7288–7310. PMLR, 2023.
- Yu, D., Huber, W., and Vitek, O. Shrinkage estimation of dispersion in negative binomial models for rna-seq experiments with small sample size. *Bioinformatics*, 29(10):1275–1282, 2013.
- Zanella, G. Informed proposals for local mcmc in discrete spaces. *Journal of the American Statistical Association*, 115(530):852–865, 2020.
- Zarfaty, L., Barkai, E., and Kessler, D. A. Discrete sampling of extreme events modifies their statistics. *Physical Review Letters*, 129(9):094101, 2022.
- Zhang, R., Li, C., Zhang, J., Chen, C., and Wilson, A. G. Cyclical stochastic gradient mcmc for bayesian deep learning. *arXiv preprint arXiv:1902.03932*, 2019.
- Zhang, R., Liu, X., and Liu, Q. A langevin-like sampler for discrete distributions. In *International Conference on Machine Learning*, pp. 26375–26396. PMLR, 2022.
- Zheng, H., Zhang, R., and Lin, G. Exploring non-convex discrete energy landscapes: A langevin-like sampler with replica exchange. *openreview.net*, 2024.
- Ziyin, L., Li, B., Simon, J. B., and Ueda, M. Sgd can converge to local maxima. In *International Conference on Learning Representations*, 2021.

A. Algorithm with Different Variables

Binary Variables When the variable domain Θ is binary, i.e., $\{0, 1\}^d$, the algorithm in Algorithm 1 can be further simplified for each chain update, which clearly shows that our method can be efficiently computed in parallel on both CPUs and GPUs.

Algorithm 2 Each chain with Binary Variables

given: Stepsize α .
loop
 compute $p(\theta) = \frac{\exp(-\frac{1}{2}\nabla U(\theta) \odot (2\theta - 1) - \frac{1}{2\alpha})}{\exp(-\frac{1}{2}\nabla U(\theta) \odot (2\theta - 1) - \frac{1}{2\alpha}) + 1}$
 sample $\mu \sim \text{Unif}(0, 1)^d$
 $I \leftarrow \text{dim}(\mu \leq p(\theta))$
 $\theta' \leftarrow \text{flipdim}(I)$
 compute $q(\theta'|\theta) = \prod_i q_i(\theta'_i|\theta) = \prod_{i \in I} p(\theta)_i \cdot \prod_{i \notin I} (1 - p(\theta)_i)$
 compute $p(\theta') = \frac{\exp(-\frac{1}{2}\nabla U(\theta') \odot (2\theta' - 1) - \frac{1}{2\alpha})}{\exp(-\frac{1}{2}\nabla U(\theta') \odot (2\theta' - 1) - \frac{1}{2\alpha}) + 1}$
 compute $q(\theta|\theta') = \prod_i q_i(\theta_i|\theta') = \prod_{i \in I} p(\theta')_i \cdot \prod_{i \notin I} (1 - p(\theta')_i)$
 set $\theta \leftarrow \theta'$ with probability in Equation (5)
end loop
output: samples $\{\theta_k\}$

Category Variables When using one-hot vectors to represent categorical variables, our discrete Langevin proposal becomes

$$\text{Categorical} \left(\text{Softmax} \left(\frac{\beta}{2} \nabla U(\theta)_i^\top (\theta'_i - \theta_i) - \frac{\|\theta'_i - \theta_i\|_p^p}{2\alpha} \right) \right),$$

where θ_i, θ'_i are one-hot vectors.

B. Iterative Tuning Algorithm

Algorithm 3 Iterative Tuning Algorithm

given: Initial temperature schedule \mathcal{T}_K of size K , tuning steps n_{\max} , sampling steps \hat{n} , and ϵ ,
for $n = 1, \dots, n_{\max}$ **do**
 $\{\hat{s}_k\}_{k=1}^{K-1} \leftarrow \text{PTDLP}(\mathcal{T}_K, \hat{n})$
 calculate points $\{(\beta_1, \hat{\Lambda}_n(\beta_1)), \dots, (\beta_K, \hat{\Lambda}_n(\beta_K))\}$ using Equation (8)
 compute $\hat{\Lambda}(\cdot)$ by using monotone piecewise cubic interpolation (Fritsch & Carlson, 1980)
 for $k = 1, \dots, K$ **do**
 find β_k^* using Equation (7) and bisection
 $\beta_k \leftarrow \beta_k^*$
 end for
 if $|\hat{\Lambda}_n - \hat{\Lambda}_{n-1}| < \epsilon$ **then**
 $\hat{\Lambda}_{n_{\max}}(\cdot) \leftarrow \hat{\Lambda}_n(\cdot)$
 break
 end if
end for
 $K^* \leftarrow \left(2 + 3\hat{\Lambda}_{n_{\max}} + \sqrt{9\hat{\Lambda}_{n_{\max}}^2 + 20\hat{\Lambda}_{n_{\max}} + 4} \right) / 4$
for $k = 1, \dots, K^*$ **do**
 find β_k^* using Equation (7) and bisection
end for
output: Optimal temperature schedule $\mathcal{T}_{K^*}^*$ and chain number K^*

C. Proofs in Section 4

In this section, we provide a proof of Section 4 in the main paper.

Proof of Theorem 4.2. We follow the proof of Syed (2022, Theorem 1) and extend to our algorithm. We define the index process for machine k as $(I_i^k, \varepsilon_i^k) \in \{1, \dots, K\} \times \{-1, 1\}$, where $\varepsilon_i^k = 1$ if the temperature parameter on machine k is proposed an increase after step i , and -1 otherwise. To simplify notation for the rest of the proof, let T_\uparrow and T_\downarrow be the hitting times to the target and reference defined by,

$$T_\uparrow = \min \{n : (I_n, \varepsilon_n) = (K, 1)\}, \quad T_\downarrow = \min \{n : (I_n, \varepsilon_n) = (0, -1)\}$$

Denote by $a_\bullet^i = \mathbb{E}(T_\bullet \mid I_0 = i)$ and $\bullet \in \{\uparrow, \downarrow\}$. Then we have

$$\mathbb{E}(T) = a_\uparrow^0 + a_\downarrow^K.$$

By using the Markov property and we have the recursion, for $k = 1, \dots, K-1$,

$$a_\bullet^k = s_k (a_\bullet^{k+1} + 1) + s_{k-1} (a_\bullet^{k-1} + 1) + (1 - s_{k-1} - s_k) (a_\bullet^k + 1)$$

Then we have $-1 = s_k (a_\bullet^{k+1} - a_\bullet^k) - s_{k-1} (a_\bullet^k - a_\bullet^{k-1})$, which implies that

$$-k + 1 = s_k (a_\bullet^{k+1} - a_\bullet^k) - s_1 (a_\bullet^2 - a_\bullet^1) \quad (11)$$

and

$$-(K - k + 1) = s_K (a_\bullet^K - a_\bullet^{K-1}) - s_{k-1} (a_\bullet^k - a_\bullet^{k-1}). \quad (12)$$

Consider that $a_\uparrow^1 = s_1 (a_\uparrow^2 + 1) + (1 - s_1) (a_\uparrow^1 + 1)$, which implies that

$$-1 = s_1 (a_\uparrow^2 - a_\uparrow^1). \quad (13)$$

Substituting Equation (13) into Equation (11) and using the fact that $a_\uparrow^K = 0$ yield $a_\uparrow^1 = \sum_{k=1}^{K-1} (k/s_k)$. Similarly, we obtain $a_\downarrow^K = \sum_{k=1}^{K-1} (K - k + 1)/s_k$. Therefore, we have

$$\mathbb{E}[T] = a_\uparrow^0 + a_\downarrow^K = (K + 1) \sum_{k=1}^{K-1} \frac{1}{s_k}. \quad (14)$$

We say a round trip has occurred on machine k when I_i^k goes from 1 to K and then goes back to 0. Note that by Assumption 4.1, the round trip \mathcal{R}_n^j is a delayed renewal process. By using the key renewal theorem, we obtain

$$\tau = \sum_{k=1}^K \lim_{i \rightarrow \infty} \frac{\mathbb{E}[\mathcal{R}_i^k]}{i} = \frac{K}{\mathbb{E}[T]}. \quad (15)$$

Substituting Equation (14) into Equation (15) yields

$$\tau(\mathcal{T}_K) = \frac{K}{\mathbb{E}[T]} = \frac{K}{(K + 1) \sum_{k=1}^{K-1} 1/s_k}.$$

□

Proof of Proposition 4.3. Recall that the round trip rate of our algorithm with \mathcal{B} copies is

$$\tau_\Lambda(K) = \frac{\mathcal{B}K}{(K + 1) \sum_{k=1}^{K-1} \frac{1}{s_k}}. \quad (16)$$

By using the fact that the swap rates are all equal, we obtain, for any $k = 1, \dots, K - 1$,

$$\sum_{k=1}^{K-1} \frac{1}{s_k} = \frac{K-1}{1 - \frac{\Lambda}{K-1}}.$$

Substituting the above equation into Equation (16) yields

$$\tau_\Lambda = \frac{\bar{K}(K-1-\Lambda)}{(K+1)(K-1)^2}. \quad (17)$$

To maximize Equation (17), we need to take the derivative and find the critical points. Denote by $f(K) := \frac{(K-1-\Lambda)}{(K+1)(K-1)^2}$ and let $f'(K) = 0$, we obtain,

$$K^* = \frac{2 + 3\Lambda + \sqrt{9\Lambda^2 + 20\Lambda + 4}}{4}.$$

Finally, by verifying the second derivative, we determine that this point corresponds to a maximum. \square

D. Proofs in Section 5.1

Lemma D.1. *If the target distribution is assumed to be log-quadratic, i.e., for any $\theta \in \Theta$, $\pi^{\beta_k}(\theta) \propto \exp(\beta_k(\theta^\top W\theta + b^\top \theta))$ with some constants³ $W \in \mathbb{R}^{d \times d}$ and $b \in \mathbb{R}^d$. Then the Markov chain following transition $q_{\alpha,k}(\cdot | \theta)$ in Equation (4) for any k is reversible with respect to some distribution $\pi_\alpha^{\beta_k}$, and $\pi_\alpha^{\beta_k}$ converges weakly to π^{β_k} as $\alpha \rightarrow 0$.*

Proof. The main idea of the proof is to replace the gradient term in the proposal by the energy difference $U(\theta') - U(\theta)$ using Taylor series approximation, and then show the reversibility of the chain based on the proofs in Zanella (2020); Zhang et al. (2022). We divide the proof into two parts. In the first part, we prove the convergence of our algorithm to $\pi_\alpha^{\beta_k}$, and in the second part, we derive the distance between $\pi_\alpha^{\beta_k}$ and π_α .

Recall that the target distribution is $\pi^{\beta_k}(\theta) = \exp(\beta_k(\theta^\top W\theta + b^\top \theta)) / Z$. We have that $\nabla \log(\pi(\theta)) = \beta_k(2W^\top \theta + b)$, $\nabla^2 \log(\pi(\theta)) = 2\beta_k W$. Then, by using the fact that $U(\theta') - U(\theta) = \nabla U(\theta)^\top (\theta' - \theta) + \frac{1}{2}(\theta' - \theta)^\top 2W(\theta' - \theta)$ by Taylor series approximation, we can rewrite the proposal distribution as the following

$$\begin{aligned} q_{\alpha}^{\beta_k}(\theta' | \theta) &= \frac{\exp\left(\frac{\beta_k}{2}\nabla U(\theta)^\top (\theta' - \theta) + \frac{\beta_k}{2}(\theta' - \theta)^\top W(\theta' - \theta) - \frac{\beta_k}{2}(\theta' - \theta)^\top W(\theta' - \theta) - \frac{1}{2\alpha}\|\theta' - \theta\|_p^p\right)}{\sum_x \exp\left(\frac{\beta_k}{2}\nabla U(\theta)^\top (x - \theta) + \frac{\beta_k}{2}(x - \theta)^\top W(x - \theta) - \frac{\beta_k}{2}(x - \theta)^\top W(x - \theta) - \frac{1}{2\alpha}\|\theta' - \theta\|_p^p\right)} \\ &= \frac{\exp\left(\frac{\beta_k}{2}(U(\theta') - U(\theta)) - \frac{\beta_k}{2}(\theta' - \theta)^\top W(\theta' - \theta) - \frac{1}{2\alpha}\|\theta' - \theta\|_p^p\right)}{\sum_x \exp\left(\frac{\beta_k}{2}(U(x) - U(\theta)) - \frac{\beta_k}{2}(x - \theta)^\top W(x - \theta) - \frac{1}{2\alpha}\|\theta' - \theta\|_p^p\right)}. \end{aligned} \quad (18)$$

Denote by $Z_\alpha^{\beta_k}(\theta) = \sum_x \exp\left(\frac{\beta_k}{2}(U(x) - U(\theta)) - \frac{\beta_k}{2}(x - \theta)^\top W(x - \theta) - \frac{1}{2\alpha}\|\theta' - \theta\|_p^p\right)$, and $\pi_\alpha^{\beta_k} = \frac{Z_\alpha^{\beta_k}(\theta)\pi^{\beta_k}(\theta)}{\sum_x Z_\alpha^{\beta_k}(x)\pi^{\beta_k}(x)}$, now we will show that $q_\alpha^{\beta_k}$ is reversible w.r.t. $\pi_\alpha^{\beta_k}$. We have that

$$\begin{aligned} \pi_\alpha^{\beta_k}(\theta)q_\alpha^{\beta_k}(\theta' | \theta) &= \frac{Z_\alpha^{\beta_k}(\theta)\pi^{\beta_k}(\theta)}{\sum_x Z_\alpha^{\beta_k}(x)\pi^{\beta_k}(x)} \frac{\exp\left(\frac{\beta_k}{2}(U(\theta') - U(\theta)) - \frac{\beta_k}{2}(\theta' - \theta)^\top W(\theta' - \theta) - \frac{1}{2\alpha}\|\theta' - \theta\|_p^p\right)}{Z_\alpha^{\beta_k}(\theta)} \\ &= \frac{\exp\left(\frac{\beta_k}{2}(U(\theta') + U(\theta)) - \frac{\beta_k}{2}(\theta' - \theta)^\top W(\theta' - \theta) - \frac{1}{2\alpha}\|\theta' - \theta\|_p^p\right)}{Z^{\beta_k} \cdot \sum_x Z_\alpha^{\beta_k}(x)\pi^{\beta_k}(x)}. \end{aligned} \quad (19)$$

³Without loss of generality, we assume W is symmetric, otherwise we can replace W with $(W + W^\top) / 2$ for the eigendecomposition.

We note that Equation (19) is symmetric in θ and θ' . Therefore $q_\alpha^{\beta_k}$ is reversible and its stationary distribution is $\pi_\alpha^{\beta_k}$. Next, we will prove that $\pi_\alpha^{\beta_k}$ converges weakly to π^{β_k} as $\alpha \rightarrow 0$. Notice that for any θ ,

$$Z_\alpha^{\beta_k}(\theta) = \sum_x \exp\left(\frac{\beta_k}{2}(U(x) - U(\theta)) - \frac{\beta_k}{2}(x - \theta)^\top W(x - \theta) - \frac{1}{2\alpha}\|\theta' - \theta\|_p^p\right) \stackrel{\alpha \downarrow 0}{=} 1$$

By Scheffé's Lemma, we attain that π_α converges weakly to π . □

Proof of Theorem 5.1. To explore the reversibility of our algorithm, we follow the proof of Zhang et al. (2022). We first consider the transition probability of the first chain (with temperature equals to one) $q_\alpha(\theta'|\theta_i^{(1)})$. Considering the presence of the swap mechanism, we write $q_\alpha(\theta'|\theta_i^{(1)})$ as follows,

$$\begin{aligned} & q_\alpha\left(\theta' \mid \theta_i^{(1)}\right) \\ &= \sum_{\theta_i^{(2)}} \sum_{\theta_{i+1}^{(2)}} \pi_\alpha^{\beta_2}\left(\theta_i^{(2)}\right) q_{\alpha,2}\left(\theta_{i+1}^{(2)} \mid \theta_i^{(2)}\right) \left[1 - s_1\left(\theta', \theta_{i+1}^{(2)}\right)\right] q_{\alpha,1}\left(\theta' \mid \theta_i^{(1)}\right) \\ &+ \sum_{\theta_i^{(3)}} \sum_{\theta_{i+1}^{(3)}} \sum_{\theta_i^{(2)}} \sum_{\theta_{i+1}^{(2)}} \pi_\alpha^{\beta_2}\left(\theta_i^{(2)}\right) q_{\alpha,2}\left(\theta' \mid \theta_i^{(2)}\right) s_1\left(\theta_{i+1}^{(1)}, \theta'\right) q_{\alpha,1}\left(\theta_{i+1}^{(1)} \mid \theta_i^{(1)}\right) \left(1 - s_2\left(\theta', \theta_{i+1}^{(3)}\right)\right) q_{\alpha,3}\left(\theta_{i+1}^{(3)} \mid \theta_i^{(3)}\right) \pi_\alpha^{\beta_3}\left(\theta_i^{(3)}\right) \\ &+ \sum_{\theta_i^{(3)}} \sum_{\theta_i^{(2)}} \sum_{\theta_{i+1}^{(2)}} \sum_{\theta_{i+1}^{(1)}} \pi_\alpha^{\beta_2}\left(\theta_i^{(2)}\right) q_{\alpha,2}\left(\theta_{i+1}^{(2)} \mid \theta_i^{(2)}\right) s_1\left(\theta_{i+1}^{(1)}, \theta'\right) q_{\alpha,1}\left(\theta_{i+1}^{(1)} \mid \theta_i^{(1)}\right) s_2\left(\theta_{i+1}^{(2)}, \theta'\right) q_{\alpha,3}\left(\theta' \mid \theta_i^{(3)}\right) \pi_\alpha^{\beta_3}\left(\theta_i^{(3)}\right). \end{aligned} \tag{20}$$

To demonstrate the reversibility, we multiply $\pi_\alpha^{\beta_1}(\theta)$ from both sides:

$$\begin{aligned} & \pi_\alpha^{\beta_1}\left(\theta_i^{(1)}\right) q_\alpha\left(\theta' \mid \theta_i^{(1)}\right) \\ &= \sum_{\theta_i^{(2)}} \sum_{\theta_{i+1}^{(2)}} \pi_\alpha^{\beta_2}\left(\theta_i^{(2)}\right) q_{\alpha,2}\left(\theta_{i+1}^{(2)} \mid \theta_i^{(2)}\right) \left[1 - s_1\left(\theta', \theta_{i+1}^{(2)}\right)\right] \pi_\alpha^{\beta_1}\left(\theta_i^{(1)}\right) q_{\alpha,1}\left(\theta' \mid \theta_i^{(1)}\right) \\ &+ \sum_{\theta_i^{(3)}} \sum_{\theta_{i+1}^{(3)}} \sum_{\theta_i^{(2)}} \sum_{\theta_{i+1}^{(2)}} \left(\pi_\alpha^{\beta_2}\left(\theta_i^{(2)}\right) q_{\alpha,2}\left(\theta' \mid \theta_i^{(2)}\right) s_1\left(\theta_{i+1}^{(1)}, \theta'\right) \pi_\alpha^{\beta_1}\left(\theta_i^{(1)}\right) q_{\alpha,1}\left(\theta_{i+1}^{(1)} \mid \theta_i^{(1)}\right)\right) \\ &\times \left(1 - s_2\left(\theta', \theta_{i+1}^{(3)}\right)\right) q_{\alpha,3}\left(\theta_{i+1}^{(3)} \mid \theta_i^{(3)}\right) \pi_\alpha^{\beta_3}\left(\theta_i^{(3)}\right) \\ &+ \sum_{\theta_i^{(3)}} \sum_{\theta_i^{(2)}} \sum_{\theta_{i+1}^{(2)}} \sum_{\theta_{i+1}^{(1)}} \pi_\alpha^{\beta_2}\left(\theta_i^{(2)}\right) q_{\alpha,2}\left(\theta_{i+1}^{(2)} \mid \theta_i^{(2)}\right) s_1\left(\theta_{i+1}^{(1)}, \theta'\right) \pi_\alpha^{\beta_1}\left(\theta_i^{(1)}\right) q_{\alpha,1}\left(\theta_{i+1}^{(1)} \mid \theta_i^{(1)}\right) \\ &\times s_2\left(\theta_{i+1}^{(2)}, \theta'\right) q_{\alpha,3}\left(\theta' \mid \theta_i^{(3)}\right) \pi_\alpha^{\beta_3}\left(\theta_i^{(3)}\right), \end{aligned}$$

where s_1 and s_2 are defined in Equation (6). Note that, by using Lemma D.1, $\pi_\alpha^{\beta_1}\left(\theta_i^{(1)}\right) q_{\alpha,1}\left(\cdot \mid \theta_i^{(1)}\right)$, $\pi_\alpha^{\beta_2}\left(\theta_i^{(2)}\right) q_{\alpha,2}\left(\cdot \mid \theta_i^{(2)}\right)$, and $\pi_\alpha^{\beta_3}\left(\theta_i^{(3)}\right) q_{\alpha,3}\left(\cdot \mid \theta_i^{(3)}\right)$ are symmetric, which indicates that $\pi_\alpha\left(\theta_i^{(1)}\right) q_\alpha\left(\theta' \mid \theta_i^{(1)}\right)$ is also symmetric. Therefore, we conclude that $q_\alpha\left(\theta' \mid \theta_i^{(1)}\right)$ in Equation (20) is reversible and the stationary distribution is $\pi_\alpha^{\beta_1}\left(\theta_i^{(1)}\right)$.

Next, to generalize the convergence result from log-quadratic distributions to general distributions, we follow the assumption in Zhang et al. (2022), i.e., we assume that $\exists W \in \mathbb{R}^{d \times d}, b \in \mathbb{R}, \epsilon \in \mathbb{R}^+, \text{ such that}$

$$\|\nabla U(\theta) - (2W\theta + b)\|_1 \leq \epsilon, \forall \theta \in \Theta.$$

Then, we consider the convergence rate with respect to step size in terms of the L_1 norm. Recall that π^{β_1} is the target distribution, $\tilde{\pi}^{\beta_1}$ is the log-quadratic distribution that is close to π^{β_1} , $\pi_\alpha^{\beta_1}$ is the stationary distribution of our algorithm without MH step. $\tilde{\pi}_\alpha^{\beta_1}$ is the stationary distribution of our algorithm targeting $\tilde{\pi}^{\beta_1}$. By using triangle inequality, we obtain

$$\left\|\pi_\alpha^{\beta_1} - \pi^{\beta_1}\right\|_1 \leq \underbrace{\left\|\pi_\alpha^{\beta_1} - \tilde{\pi}_\alpha^{\beta_1}\right\|_1}_{\mathfrak{I}_1} + \underbrace{\left\|\tilde{\pi}_\alpha^{\beta_1} - \tilde{\pi}^{\beta_1}\right\|_1}_{\mathfrak{I}_2} + \underbrace{\left\|\tilde{\pi}^{\beta_1} - \pi^{\beta_1}\right\|_1}_{\mathfrak{I}_3}.$$

For \mathfrak{T}_3 , let the energy function of $\tilde{\pi}^{\beta_1}$ be $\beta_1 V(\theta) = \beta_1(\theta^\top W\theta + b\theta)$. Since Θ is a discrete space, there exists a bounded subset $\Omega \in \mathbb{R}^d$ such that Θ is a subset of Ω . By Poincaré inequality, we get

$$\|U(\theta) - V(\theta)\| \leq C_1 \cdot \|\nabla U(\theta) - (W\theta + b)\|_1 \leq C_1\epsilon, \quad \forall \theta \in \Theta,$$

where the constant C_1 depends on Ω . Recall that $\pi^{\beta_1}(\theta) = \frac{\exp(\beta_1 U(\theta))}{Z^{\beta_1}}$ and $\tilde{\pi}^{\beta_1}(\theta) = \frac{\exp(\beta_1 V(\theta))}{\tilde{Z}^{\beta_1}}$, where \tilde{Z}^{β_1} is the normalizing constant to make $\tilde{\pi}^{\beta_1}$ a distribution. Then

$$\left\| \pi^{\beta_1} - \tilde{\pi}^{\beta_1} \right\|_1 = \sum_{\theta \in \Theta} \left| \frac{\exp(\beta_1 U(\theta))}{Z^{\beta_1}} - \frac{\exp(\beta_1 V(\theta))}{\tilde{Z}^{\beta_1}} \right|. \quad (21)$$

We notice that, for any θ ,

$$\frac{\exp(\beta_1 U(\theta))}{\exp(\beta_1 V(\theta))} = \exp(\beta_1(U(\theta) - V(\theta))) \leq \exp(\beta_1|U(\theta) - V(\theta)|) \leq \exp(\beta_1 C_1\epsilon)$$

and similarly $\frac{\exp(\beta_1 V(\theta))}{\exp(\beta_1 U(\theta))} \leq \exp(\beta_1 C_1\epsilon)$. Therefore we have, for any θ ,

$$\begin{aligned} \left| \frac{\exp(\beta_1 U(\theta))}{Z^{\beta_1}} - \frac{\exp(\beta_1 V(\theta))}{\tilde{Z}^{\beta_1}} \right| &\leq (\exp(\beta_1 C_1\epsilon) - 1) \max \left\{ \frac{\exp(\beta_1 U(\theta))}{Z^{\beta_1}}, \frac{\exp(\beta_1 V(\theta))}{\tilde{Z}^{\beta_1}} \right\} \\ &\leq (\exp(\beta_1 C_1\epsilon) - 1) \left(\frac{\exp(\beta_1 U(\theta))}{Z^{\beta_1}} + \frac{\exp(\beta_1 V(\theta))}{\tilde{Z}^{\beta_1}} \right) \end{aligned}$$

Plugging the above in Equation (21), we obtain

$$\left\| \pi^{\beta_1} - \tilde{\pi}^{\beta_1} \right\|_1 \leq 2(\exp(\beta_1 C_1\epsilon) - 1). \quad (22)$$

For \mathfrak{T}_2 ,

$$\left\| \tilde{\pi}_\alpha^{\beta_1} - \tilde{\pi}^{\beta_1} \right\|_1 = \sum_{\theta} \left| \frac{Z_\alpha^{\beta_1}(\theta) \tilde{\pi}^{\beta_1}(\theta)}{\sum_x Z_\alpha^{\beta_1}(x) \tilde{\pi}^{\beta_1}(x)} - \tilde{\pi}^{\beta_1}(\theta) \right|.$$

For each absolute value term, we have

$$\begin{aligned} &\left| \frac{\tilde{Z}_\alpha^{\beta_1}(\theta) \tilde{\pi}^{\beta_1}(\theta)}{\sum_x \tilde{Z}_\alpha^{\beta_1}(x) \tilde{\pi}^{\beta_1}(x)} - \tilde{\pi}^{\beta_1}(\theta) \right| \\ &= \tilde{\pi}^{\beta_1}(\theta) \left| \frac{1 + \sum_{x \neq \theta} \exp\left(\frac{\beta_1}{2}(V(x) - V(\theta)) - \frac{\beta_1}{2}(x - \theta)^\top W(x - \theta) - \frac{1}{2\alpha} \|\theta' - \theta\|_p^p\right)}{1 + \sum_x \frac{1}{\tilde{Z}_\alpha^{\beta_1}} \exp(\beta_1 V(x)) \sum_{y \neq x} \exp\left(\frac{\beta_1}{2}(V(y) - V(x)) - \frac{\beta_1}{2}(y - x)^\top W(y - x) - \frac{1}{2\alpha} \|\theta' - \theta\|_p^p\right)} - 1 \right|. \end{aligned}$$

By using the fact that $x^\top Wx \geq \lambda_{\min}(W)\|x\|^2, \forall x$, it follows that,

$$\frac{\beta_1}{2}(x - \theta)^\top W(x - \theta) \geq \frac{\beta_1 \lambda_{\min}}{2} \|x - \theta\|^2.$$

We also notice that $\min_{x \neq \theta} \|x - \theta\| = 1$, thus when $\frac{\tilde{Z}_\alpha^{\beta_1}(\theta)}{\sum_x \tilde{Z}_\alpha^{\beta_1}(x) \tilde{\pi}^{\beta_1}(x)} - 1 > 0$, we get

$$\begin{aligned} &\left| \frac{\tilde{Z}_\alpha^{\beta_1}(\theta) \tilde{\pi}^{\beta_1}(\theta)}{\sum_x \tilde{Z}_\alpha^{\beta_1}(x) \tilde{\pi}^{\beta_1}(x)} - \tilde{\pi}^{\beta_1}(\theta) \right| \\ &= \tilde{\pi}^{\beta_1}(\theta) \left(\frac{1 + \sum_{x \neq \theta} \exp\left(\frac{\beta_1}{2}(V(x) - V(\theta)) - \frac{\beta_1}{2}(x - \theta)^\top W(x - \theta) - \frac{1}{2\alpha} \|\theta' - \theta\|_p^p\right)}{1 + \sum_y \frac{1}{\tilde{Z}_\alpha^{\beta_1}} \exp(\beta_1 V(y)) \sum_{x \neq y} \exp\left(\frac{\beta_1}{2}(V(x) - V(y)) - \frac{\beta_1}{2}(x - y)^\top W(x - y) - \frac{1}{2\alpha} \|\theta' - \theta\|_p^p\right)} - 1 \right) \\ &\leq \tilde{\pi}^{\beta_1}(\theta) \left(1 + \sum_{x \neq \theta} \exp\left(\frac{\beta_1}{2}(V(x) - V(\theta)) - \frac{\beta_1 \lambda_{\min}}{2} \|x - \theta\|^2 - \frac{1}{2\alpha} \|x - \theta\|_p^p\right) - 1 \right) \\ &\leq \tilde{\pi}^{\beta_1}(\theta) \left(\sum_{x \neq \theta} \exp\left(\frac{\beta_1}{2}(V(x) - V(\theta))\right) \right) \cdot \exp\left(-\frac{1 + \alpha \beta_1 \lambda_{\min}}{2\alpha}\right) \\ &= \tilde{\pi}^{\beta_1}(\theta) \left(\sum_x \exp\left(\frac{\beta_1}{2} V(x)\right) \right) \exp(-\beta_1 V(\theta)) \cdot \exp\left(-\frac{1 + \alpha \beta_1 \lambda_{\min}}{2\alpha}\right) \\ &= \left(\sum_x \exp\left(\frac{\beta_1}{2} V(x)\right) / \tilde{Z}^{\beta_1} \right) \cdot \exp\left(-\frac{1 + \alpha \beta_1 \lambda_{\min}}{2\alpha}\right). \end{aligned}$$

Then, we obtain,

$$\sum_{\theta} \left| \frac{\tilde{Z}_{\alpha}^{\beta_1}(\theta) \tilde{\pi}^{\beta_1}(\theta)}{\sum_x \tilde{Z}_{\alpha}^{\beta_1}(x) \tilde{\pi}(x)} - \tilde{\pi}^{\beta_1}(\theta) \right| \leq \left(\sum_{\theta} 1 \right) \left(\sum_x \exp\left(\frac{\beta_1}{2} V(x)\right) / \tilde{Z}^{\beta_1} \right) \exp\left(-\frac{1 + \alpha\beta_1 \lambda_{\min}}{2\alpha}\right)$$

Similarly, when $\frac{Z_{\alpha}^{\beta_1}(\theta)}{\sum_x Z_{\alpha}^{\beta_1}(x) \pi^{\beta_1}(x)} - 1 < 0$, we have,

$$\begin{aligned} & \left| \frac{\tilde{Z}_{\alpha}^{\beta_1}(\theta) \tilde{\pi}^{\beta_1}(\theta)}{\sum_x \tilde{Z}_{\alpha}^{\beta_1}(x) \tilde{\pi}^{\beta_1}(x)} - \tilde{\pi}^{\beta_1}(\theta) \right| \\ &= \tilde{\pi}^{\beta_1}(\theta) \left(1 - \frac{1 + \sum_{x \neq \theta} \exp\left(\frac{\beta_1}{2} V(x) - \frac{\beta_1}{2} V(\theta) - \frac{\beta_1}{2} (x - \theta)^{\top} W(x - \theta) - \frac{1}{2\alpha} \|\theta' - \theta\|_p^p\right)}{1 + \sum_y \frac{1}{\tilde{Z}} \exp(V(y)) \sum_{x \neq y} \exp\left(\frac{\beta_1}{2} V(x) - \frac{\beta_1}{2} V(y) - \frac{\beta_1}{2} (x - y)^{\top} W(x - y) - \frac{1}{2\alpha} \|\theta' - \theta\|_p^p\right)} \right) \\ &\leq \tilde{\pi}^{\beta_1}(\theta) \left(1 - \frac{1}{1 + \sum_y \frac{1}{\tilde{Z}^{\beta_1}} \exp(\beta_1 V(y)) \sum_{x \neq y} \exp\left(\frac{\beta_1}{2} V(x) - \frac{\beta_1}{2} V(y) - \frac{1 + \alpha\beta_1 \lambda_{\min}}{2\alpha}\right)} \right) \\ &= \tilde{\pi}^{\beta_1}(\theta) \left(\frac{\sum_y \frac{1}{\tilde{Z}^{\beta_1}} \exp(\beta_1 V(y)) \sum_{x \neq y} \exp\left(\frac{\beta_1}{2} V(x) - \frac{\beta_1}{2} V(y) - \frac{1 + \alpha\beta_1 \lambda_{\min}}{2\alpha}\right)}{1 + \sum_y \frac{1}{\tilde{Z}^{\beta_1}} \exp(\beta_1 V(y)) \sum_{x \neq y} \exp\left(\frac{\beta_1}{2} V(x) - \frac{\beta_1}{2} V(y) - \frac{1 + \alpha\beta_1 \lambda_{\min}}{2\alpha}\right)} \right) \\ &\leq \tilde{\pi}^{\beta_1}(\theta) \left(\sum_y \frac{1}{\tilde{Z}^{\beta_1}} \exp(\beta_1 V(y)) \sum_x \exp\left(\frac{\beta_1}{2} V(x) - \frac{\beta_1}{2} V(y)\right) \right) \exp\left(-\frac{1 + \alpha\beta_1 \lambda_{\min}}{2\alpha}\right) \\ &\leq \tilde{\pi}^{\beta_1}(\theta) \sum_x \exp\left(\frac{\beta_1}{2} V(x)\right) \left(\sum_y \frac{1}{\tilde{Z}^{\beta_1}} \exp\left(\beta_1 V(y) - \frac{\beta_1}{2} V(y)\right) \right) \exp\left(-\frac{1 + \alpha\beta_1 \lambda_{\min}}{2\alpha}\right) \\ &= \tilde{\pi}^{\beta_1}(\theta) \left(\sum_x \exp\left(\frac{\beta_1}{2} V(x)\right) \right)^2 \exp\left(-\frac{1 + \alpha\beta_1 \lambda_{\min}}{2\alpha}\right) / \tilde{Z}^{\beta_1}. \end{aligned}$$

Then, we obtain,

$$\sum_{\theta} \left| \frac{\tilde{Z}_{\alpha}^{\beta_1}(\theta) \tilde{\pi}^{\beta_1}(\theta)}{\sum_x \tilde{Z}_{\alpha}^{\beta_1}(x) \tilde{\pi}(x)} - \tilde{\pi}^{\beta_1}(\theta) \right| \leq \frac{\left(\sum_x \exp\left(\frac{\beta_1}{2} V(x)\right) \right)^2}{\tilde{Z}^{\beta_1}} \exp\left(-\frac{1 + \alpha\beta_1 \lambda_{\min}}{2\alpha}\right).$$

Therefore, the difference between π_{α} and π can be bounded as follows

$$\left\| \tilde{\pi}_{\alpha}^{\beta_1} - \tilde{\pi}^{\beta_1} \right\|_1 \leq \frac{\left(\sum_x \exp\left(\frac{\beta_1}{2} V(x)\right) \right)^2}{\tilde{Z}^{\beta_1}} \exp\left(-\frac{1 + \alpha\beta_1 \lambda_{\min}}{2\alpha}\right). \quad (23)$$

For $\tilde{\mathcal{X}}_1$, let $P_{\alpha}, \tilde{P}_{\alpha}$ be the transition matrices of PTDL without MH targeting π^{β_1} and $\tilde{\pi}^{\beta_1}$. We consider the difference between these two matrices.

$$\left\| P_{\alpha} - \tilde{P}_{\alpha} \right\|_{\infty} = \max_{\theta'} \sum_{\theta} \left| \frac{\exp\left(\frac{1}{2} \nabla U(\theta)^{\top} (\theta' - \theta) - \frac{1}{2\alpha} \|\theta' - \theta\|_p^p\right)}{Z_{\alpha}^{\beta}(\theta)} - \frac{\exp\left(\frac{1}{2} \nabla V(\theta)^{\top} (\theta' - \theta) - \frac{1}{2\alpha} \|\theta' - \theta\|_p^p\right)}{\tilde{Z}_{\alpha}^{\beta}(\theta)} \right|,$$

where

$$Z_{\alpha}^{\beta}(\theta) = \sum_x \exp\left(\frac{1}{2} \nabla U(\theta)^{\top} (x - \theta) - \frac{1}{2\alpha} \|x - \theta\|_p^p\right), \quad \tilde{Z}_{\alpha}^{\beta}(\theta) = \sum_x \exp\left(\frac{1}{2} \nabla V(\theta)^{\top} (x - \theta) - \frac{1}{2\alpha} \|x - \theta\|_p^p\right).$$

We denote $\mathcal{D} = \max_{\theta, \theta' \in \Theta} \|\theta' - \theta\|_\infty$. By the assumption $\|\nabla U(\theta) - \nabla V(\theta)\|_1 \leq \epsilon$, we have

$$\begin{aligned} & \left| \frac{\exp\left(\frac{\beta_1}{2} \nabla U(\theta)^\top (\theta' - \theta) - \frac{1}{2\alpha} \|\theta' - \theta\|_p^p\right)}{Z_\alpha^{\beta_1}} - \frac{\exp\left(\frac{\beta_1}{2} \nabla V(\theta)^\top (\theta' - \theta) - \frac{1}{2\alpha} \|\theta' - \theta\|_p^p\right)}{\tilde{Z}_\alpha^{\beta_1}(\theta)} \right| \\ & \leq (\exp(\mathcal{D}\epsilon) - 1) \\ & \quad \times \max \left\{ \frac{\exp\left(\frac{1}{2} \nabla U(\theta)^\top (\theta' - \theta) - \frac{1}{2\alpha} \|\theta' - \theta\|_p^p\right)}{Z_\alpha^{\beta_1}(\theta)}, \frac{\exp\left(\frac{1}{2} \nabla V(\theta)^\top (\theta' - \theta) - \frac{1}{2\alpha} \|\theta' - \theta\|_p^p\right)}{\tilde{Z}_\alpha^{\beta_1}(\theta)} \right\} \\ & \leq (\exp(\mathcal{D}\epsilon) - 1) \\ & \quad \times \left(\frac{\exp\left(\frac{1}{2} \nabla U(\theta)^\top (\theta' - \theta) - \frac{1}{2\alpha} \|\theta' - \theta\|_p^p\right)}{Z_\alpha^{\beta_1}(\theta)} + \frac{\exp\left(\frac{1}{2} \nabla V(\theta)^\top (\theta' - \theta) - \frac{1}{2\alpha} \|\theta' - \theta\|_p^p\right)}{\tilde{Z}_\alpha^{\beta_1}(\theta)} \right). \end{aligned}$$

Then, we have

$$\|P - \tilde{P}\|_\infty \leq 2(\exp(\mathcal{D}\epsilon) - 1)$$

By using the perturbation bound in Schweitzer (1968), we obtain

$$\left\| \pi_\alpha^{\beta_1} - \tilde{\pi}_\alpha^{\beta_1} \right\|_1 \leq C_2 \cdot \left\| P_\alpha - \tilde{P}_\alpha \right\|_\infty = 2C_2(\exp(\mathcal{D}\epsilon) - 1) \quad (24)$$

where C_2 is a constant depending on $\tilde{\pi}^{\beta_1}$ and α . Combining Equations (22) to (24), we have

$$\begin{aligned} & \left\| \pi_\alpha^{\beta_1} - \tilde{\pi}_\alpha^{\beta_1} \right\|_1 \\ & \leq \left\| \pi_\alpha^{\beta_1} - \tilde{\pi}_\alpha^{\beta_1} \right\|_1 + \left\| \tilde{\pi}_\alpha^{\beta_1} - \tilde{\pi}^{\beta_1} \right\|_1 + \left\| \tilde{\pi}^{\beta_1} - \pi^{\beta_1} \right\|_1 \\ & \leq 2C_2(\exp(\mathcal{D}\epsilon) - 1) + 2(\exp(\beta_1 C_1 \epsilon) - 1) + \frac{(\sum_x \exp(\frac{\beta_1}{2} V(x)))^2}{\tilde{Z}^{\beta_1}} \exp\left(-\frac{1 + \alpha\beta_1 \lambda_{\min}}{2\alpha}\right) \\ & \leq Z_1 (\exp(Z_2 \epsilon) - 1) + Z_3 \exp\left(-\frac{1 + \alpha\beta_1 \lambda_{\min}}{2\alpha}\right), \end{aligned}$$

where we denote by $Z_1 := 2(C_2 + 1)$, $Z_2 := \mathcal{D} + \beta_1 C_1$, and $Z_3 := (\sum_x \exp(\frac{\beta_1}{2} V(x)))^2 / \tilde{Z}^{\beta_1}$. \square

Proof of Theorem 5.2. Recall Equation (20), we have

$$\begin{aligned} & \sum_{\theta' \neq \theta_i^{(1)}} q_\alpha(\theta' | \theta_i^{(1)}) \\ & = \sum_{\theta' \neq \theta_i^{(1)}} \sum_{\theta_i^{(2)}} \sum_{\theta_{i+1}^{(2)}} \pi_\alpha^{\beta_2}(\theta_i^{(2)}) q_{\alpha,2}(\theta_{i+1}^{(2)} | \theta_i^{(2)}) \left[1 - s_1(\theta', \theta_{i+1}^{(2)})\right] q_{\alpha,1}(\theta' | \theta_i^{(1)}) \\ & \quad + \sum_{\theta' \neq \theta_i^{(1)}} \sum_{\theta_i^{(3)}} \sum_{\theta_{i+1}^{(3)}} \sum_{\theta_i^{(2)}} \sum_{\theta_{i+1}^{(1)}} \pi_\alpha^{\beta_2}(\theta_i^{(2)}) q_{\alpha,2}(\theta' | \theta_i^{(2)}) s_1(\theta_{i+1}^{(1)}, \theta') q_{\alpha,1}(\theta_{i+1}^{(1)} | \theta_i^{(1)}) (1 - s_2(\theta', \theta_{i+1}^{(3)})) q_{\alpha,3}(\theta_{i+1}^{(3)} | \theta_i^{(3)}) \pi_\alpha^{\beta_3}(\theta_i^{(3)}) \\ & \quad + \sum_{\theta' \neq \theta_i^{(1)}} \sum_{\theta_i^{(3)}} \sum_{\theta_i^{(2)}} \sum_{\theta_{i+1}^{(2)}} \sum_{\theta_{i+1}^{(1)}} \pi_\alpha^{\beta_2}(\theta_i^{(2)}) q_{\alpha,2}(\theta_{i+1}^{(2)} | \theta_i^{(2)}) s_1(\theta_{i+1}^{(1)}, \theta') q_{\alpha,1}(\theta_{i+1}^{(1)} | \theta_i^{(1)}) s_2(\theta_{i+1}^{(2)}, \theta') q_{\alpha,3}(\theta' | \theta_i^{(3)}) \pi_\alpha^{\beta_3}(\theta_i^{(3)}) \\ & \leq \sum_{\theta' \neq \theta_i^{(1)}} \left(q_{\alpha,1}(\theta' | \theta_i^{(1)}) + \sum_{\theta_i^{(2)}} \pi_\alpha^{\beta_2}(\theta_i^{(2)}) q_{\alpha,2}(\theta' | \theta_i^{(2)}) + \sum_{\theta_i^{(3)}} \pi_\alpha^{\beta_3}(\theta_i^{(3)}) q_{\alpha,3}(\theta' | \theta_i^{(3)}) \right) \\ & \leq \sum_{\theta' \neq \theta_i^{(1)}} q_{\alpha,1}(\theta' | \theta_i^{(1)}) + 2 \end{aligned} \quad (25)$$

By using Equation (18) and letting $\beta_1 = 1$, we have

$$\begin{aligned}
 q_{\alpha,1}(\theta' | \theta) &= \frac{\exp\left(\frac{1}{2}(U(\theta') - U(\theta)) - \frac{1}{2}(\theta' - \theta)^\top W(\theta' - \theta) - \frac{1}{2\alpha}\|\theta' - \theta\|_p^p\right)}{\sum_x \exp\left(\frac{1}{2}(U(x) - U(\theta)) - \frac{1}{2}(x - \theta)^\top W(x - \theta) - \frac{1}{2\alpha}\|\theta' - \theta\|_p^p\right)} \\
 &= \frac{\exp\left(\frac{1}{2}(U(\theta') - U(\theta)) - \frac{1}{2}(\theta' - \theta)^\top W(\theta' - \theta) - \frac{1}{2\alpha}\|\theta' - \theta\|_p^p\right)}{1 + \sum_{x \neq \theta} \exp\left(\frac{1}{2}(U(x) - U(\theta)) - \frac{1}{2}(x - \theta)^\top W(x - \theta) - \frac{1}{2\alpha}\|\theta' - \theta\|_p^p\right)} \\
 &\leq \exp\left\{\frac{1}{2}(U(\theta') - U(\theta)) - \frac{1}{2}(\theta' - \theta)^\top W(\theta' - \theta) - \frac{1}{2\alpha}\|\theta' - \theta\|_p^p\right\}.
 \end{aligned} \tag{26}$$

By substituting Equation (26) into Equation (25) and the fact that $\frac{x^\top W x}{x^\top x} \geq \lambda_{\min}(W)$ for any $x \neq 0$, one writes

$$\begin{aligned}
 \sum_{\theta' \neq \theta_i^{(1)}} q_\alpha(\theta' | \theta_i^{(1)}) &\leq \sum_{\theta' \neq \theta_i^{(1)}} \exp\left\{\frac{1}{2}(U(\theta') - U(\theta_i^{(1)})) - \frac{1}{2}(\theta' - \theta_i^{(1)})^\top W(\theta' - \theta_i^{(1)}) - \frac{1}{2\alpha}\|\theta' - \theta_i^{(1)}\|_p^p\right\} + 2 \\
 &\leq 2 \sum_{\theta'} \exp\left\{\frac{1}{2}(U(\theta') - U(\theta_i^{(1)})) - \frac{1}{2}(\theta' - \theta_i^{(1)})^\top W(\theta' - \theta_i^{(1)}) - \frac{1}{2\alpha}\|\theta' - \theta_i^{(1)}\|_p^p\right\} \\
 &\leq 2 \sum_{\theta'} \exp\left\{\frac{1}{2}(U(\theta') - U(\theta_i^{(1)})) - \frac{1}{2}\lambda_{\min}(W)\mathcal{D}^2 - \frac{1}{2\alpha}\mathcal{D}^p\right\} \\
 &\leq 2 \exp\left\{-\frac{1}{2}\lambda_{\min}(W)\mathcal{D}^2 - \frac{1}{2\alpha}\mathcal{D}^p\right\} \sum_{\theta'} \exp\left\{\frac{1}{2}(U(\theta') - U(\theta_i^{(1)}))\right\} \\
 &\leq 2Z \exp\left\{-\frac{1}{2}\lambda_{\min}(W)\mathcal{D}^2 - \frac{1}{2\alpha}\mathcal{D}^p\right\},
 \end{aligned}$$

where Z is the normalizing constant of the target distribution π . Note that q_α is reversible and the transition matrix of a reversible Markov chain has only real eigenvalues. By using [Horn & Johnson \(2012, Theorem 6.1.1\)](#), there at least exists one $\theta \in \Theta$ such that

$$|\lambda_2 - q_\alpha(\theta | \theta)| \leq Z \exp\left(-\frac{1}{2}\lambda_{\min}(W)\mathcal{D}^2 - \frac{1}{2\alpha}\mathcal{D}^p\right),$$

where λ_2 is the second largest eigenvalue of the transition matrix. Then we consider the spectral gap ([Levin & Peres, 2017, Chaper 12](#)),

$$\begin{aligned}
 1 - \lambda_2 &\leq |1 - q_\alpha(\theta | \theta)| + |q_\alpha(\theta | \theta) - \lambda_2| \\
 &\leq |1 - q_\alpha(\theta | \theta)| + 2Z \exp\left(-\frac{1}{2}\lambda_{\min}(A)d_2 - \frac{1}{2\alpha}d_p\right) \\
 &= \sum_{\theta' \neq \theta} q_\alpha(\theta' | \theta) + 2Z \exp\left(-\frac{1}{2}\lambda_{\min}(W)\mathcal{D}^2 - \frac{1}{2\alpha}\mathcal{D}^p\right) \\
 &\leq 4 \cdot Z \exp\left(-\frac{1}{2}\lambda_{\min}(W)\mathcal{D}^2 - \frac{1}{2\alpha}\mathcal{D}^p\right).
 \end{aligned} \tag{27}$$

Denote by $t_{\text{mix}}(\varepsilon) := \min\{t : d(t) \leq \varepsilon\}$ with $d(t) := \max_{\theta \in \Theta} \|P_\alpha(\theta, \cdot) - \pi_\alpha\|_{\text{TV}}$. By using [Levin & Peres \(2017, Theorem 12.5\)](#) and Equation (27), we obtain

$$\begin{aligned}
 t_{\text{mix}}(\varepsilon) &\geq \left(\frac{1}{1 - \lambda_2} - 1\right) \log\left(\frac{1}{2\varepsilon}\right) \\
 &\geq \left(\frac{1}{4 \cdot Z} \exp\left(\frac{1}{2}\lambda_{\min}(W)\mathcal{D}^2 + \frac{1}{2\alpha}\mathcal{D}^p\right) - 1\right) \log\left(\frac{1}{2\varepsilon}\right).
 \end{aligned}$$

□

E. Proofs in Section 5.2

We define the problem setting in more detail. We have a target that is of the form

$$\pi(\theta) = \frac{1}{Z} \exp(U(\theta)).$$

We consider the proposal kernel as

$$q(\theta' | \theta) \propto \exp \left\{ \beta \nabla U(\theta)^\top (\theta' - \theta) - \frac{1}{2\alpha} \|\theta' - \theta\|_p^p \right\}$$

and consider the transition kernel as

$$p(\theta' | \theta) = \left(\frac{\pi(\theta') q(\theta | \theta')}{\pi(\theta) q(\theta' | \theta)} \wedge 1 \right) q(\theta' | \theta) + (1 - L(\theta)) \delta_\theta(\theta'),$$

where

$$L(\theta) = \sum_{\theta' \in \Theta} \min \left\{ \frac{\pi(\theta') q(\theta | \theta')}{\pi(\theta) q(\theta' | \theta)}, 1 \right\} q(\theta' | \theta)$$

is the total rejection probability from θ . Finally, recall that the total variation distance between two probability measures μ and ν , defined on some space $\Theta \subset \mathbb{R}^d$ is

$$\|\mu - \nu\|_{TV} = \sup_{A \in \mathcal{B}(\Theta)} |\mu(A) - \nu(A)|,$$

where $\mathcal{B}(\Theta)$ is the set of all measurable sets in Θ .

Lemma E.1. *Let Assumptions 5.3 and 5.4 hold. Then we have, for any $\theta, \theta' \in \Theta$,*

$$p(\theta' | \theta) \geq \epsilon_{\beta, \alpha} \frac{\exp \{ \beta U(\theta') \}}{\sum_{\theta' \in \Theta} \exp \{ \beta U(\theta') \}},$$

where

$$\epsilon_{\beta, \alpha} = \exp \left\{ -\beta \left(M - \frac{m}{2} \right) \tilde{\mathcal{D}}(\Theta)^2 - \beta \|\nabla U(a)\| \tilde{\mathcal{D}}(\Theta) - \frac{1}{\alpha} \tilde{\mathcal{D}}(\Theta)^p \right\}$$

with $a \in \arg \min_{\theta \in \Theta} \|\nabla U(\theta)\|$.

Proof. We start by noting that

$$q(\theta' | \theta) = \frac{\exp \{ \beta \nabla U(\theta)^\top (\theta' - \theta) - \frac{1}{2\alpha} \|\theta' - \theta\|_p^p \}}{\sum_{\theta' \in \Theta} \exp \{ \beta \nabla U(\theta)^\top (\theta' - \theta) - \frac{1}{2\alpha} \|\theta' - \theta\|_p^p \}}. \quad (28)$$

Consider the term,

$$\beta \nabla U(\theta)^\top (\theta' - \theta) = \beta (-U(\theta) + U(\theta')) - \frac{\beta}{2} (\theta - \theta')^\top \left(\int_0^1 \nabla^2 U((1-s)\theta + s\theta') ds \right) (\theta - \theta'). \quad (29)$$

Plugging Equation (29) into Equation (28) yields the numerator of $q(\theta, \theta')$

$$\begin{aligned} & \beta \nabla U(\theta)^\top (\theta' - \theta) - \frac{1}{2\alpha} \|\theta' - \theta\|_p^p \\ &= \beta (-U(\theta) + U(\theta')) - \frac{\beta}{2} (\theta - \theta')^\top \left(\int_0^1 \nabla^2 U((1-s)\theta + s\theta') ds \right) (\theta - \theta') - \frac{1}{2\alpha} \|\theta' - \theta\|_p^p. \end{aligned}$$

By using Assumption 5.3, we have

$$\beta \int_0^1 \nabla^2 U((1-s)\theta + s\theta') ds (\theta - \theta') \geq -\beta M.$$

Since $\alpha < 1/\beta M$, the matrix $(\frac{1}{\alpha} - \beta M)I$ is positive definite. We note that

$$p(\theta' | \theta) \geq \left(\frac{\pi(\theta') q(\theta | \theta')}{\pi(\theta) q(\theta' | \theta)} \wedge 1 \right) q(\theta' | \theta) = \left(\frac{Z_{\alpha, \beta}(\theta)}{Z_{\alpha, \beta}(\theta')} \wedge 1 \right) q(\theta' | \theta), \quad (30)$$

where

$$Z_{\alpha,\beta}(\theta) = \sum_{x \in \Theta} \exp \left\{ -\beta (U(\theta) - U(x)) - \frac{1}{2} (\theta - x)^\top \left(\beta \int_0^1 \nabla^2 U((1-s)\theta + sx) ds \right) (\theta - x) - \frac{1}{2\alpha} \|\theta' - \theta\|_p^p \right\}.$$

We define $\text{conv}(\Theta)$ as the convex hull of the set Θ . Since Assumption 5.3 holds in this setting, we have an $m > 0$ such that for any $\theta \in \text{conv}(\Theta)$, $-\nabla^2 U(\theta) \geq mI$. From this, one notes that

$$\exp \left(-\beta U(\theta) + \frac{1}{2} \beta m \tilde{\mathcal{D}}(\Theta)^2 - \frac{1}{2\alpha} \tilde{\mathcal{D}}(\Theta)^p \right) \leq \frac{Z_{\alpha,\beta}(\theta)}{\sum_{x \in \Theta} \exp(\beta U(x))} \leq \exp(-\beta U(\theta)).$$

where the right-hand side follows from the fact that $\alpha < 1/(\beta M)$. Therefore,

$$\frac{Z_{\alpha,\beta}(\theta)}{Z_{\alpha,\beta}(\theta')} \geq \frac{\exp\{\beta(-U(\theta) + U(\theta'))\}}{\exp\left\{\frac{1}{2} \left(\frac{1}{\alpha} \tilde{\mathcal{D}}(\Theta)^p - \beta m \tilde{\mathcal{D}}(\Theta)^2 \right)\right\}}. \quad (31)$$

We also note that

$$\begin{aligned} q(\theta'|\theta) &= \frac{\exp\left\{\beta(-U(\theta) + U(\theta')) - (\theta - \theta')^\top \left(\frac{\beta}{2} \int_0^1 \nabla^2 U((1-s)\theta + s\theta') \right) (\theta - \theta') - \frac{1}{2\alpha} \|\theta' - \theta\|_p^p\right\}}{\sum_{\theta' \in \Theta} \exp\left\{\beta(-U(\theta) + U(\theta')) - (\theta - \theta')^\top \left(\frac{\beta}{2} \int_0^1 \nabla^2 U((1-s)\theta + s\theta') \right) (\theta - \theta') - \frac{1}{2\alpha} \|\theta' - \theta\|_p^p\right\}} \\ &\geq \frac{\exp\left\{\beta(\nabla U(\theta), \theta' - \theta) - \frac{1}{2\alpha} \|\theta' - \theta\|_p^p\right\}}{\sum_{\theta' \in \Theta} \exp\{\beta(-U(\theta) + U(\theta'))\}}. \end{aligned} \quad (32)$$

We also note that

$$\begin{aligned} -\beta(\nabla U(\theta), \theta' - \theta) + \frac{1}{2\alpha} \|\theta' - \theta\|_p^p &= \beta(-\nabla U(\theta) + \nabla U(a), \theta' - \theta) + \beta(-\nabla U(a), \theta' - \theta) + \frac{1}{2\alpha} \|\theta' - \theta\|_p^p \\ &\leq \beta(-\nabla U(\theta) + \nabla U(a), \theta' - \theta) + \beta(-\nabla U(a), \theta' - \theta) + \frac{1}{2\alpha} \tilde{\mathcal{D}}(\Theta)^p \\ &\leq \beta \|\nabla U(\theta) - \nabla U(a)\| \|\theta' - \theta\| + \beta \|\nabla U(a)\| \|\theta' - \theta\| + \frac{1}{2\alpha} \tilde{\mathcal{D}}(\Theta)^p \\ &\leq \beta \|\nabla U(\theta) - \nabla U(a)\| \tilde{\mathcal{D}}(\Theta) + \beta \|\nabla U(a)\| \tilde{\mathcal{D}}(\Theta) + \frac{1}{2\alpha} \tilde{\mathcal{D}}(\Theta)^p \\ &\leq \beta M \tilde{\mathcal{D}}(\Theta)^2 + \beta \|\nabla U(a)\| \tilde{\mathcal{D}}(\Theta) + \frac{1}{2\alpha} \tilde{\mathcal{D}}(\Theta)^p. \end{aligned} \quad (33)$$

Combining Equations (30) to (33), we obtain

$$p(\theta'|\theta) \geq \epsilon_{\beta,\alpha} \frac{\exp\{\beta U(\theta')\}}{\sum_{\theta' \in \Theta} \exp\{\beta U(\theta')\}}$$

where

$$\epsilon_{\beta,\alpha} = \exp \left\{ - \left(\beta M - \frac{\beta m}{2} \right) \tilde{\mathcal{D}}(\Theta)^2 - \beta \|\nabla U(a)\| \tilde{\mathcal{D}}(\Theta) - \frac{1}{\alpha} \tilde{\mathcal{D}}(\Theta)^p \right\}.$$

□

Since the state space is finite, for any $\theta \in \Theta$, we can denote the maximum and minimum values of $U(\theta)$ as L and l , respectively. Therefore, for any $k = 1, \dots, K-1$, we obtain

$$\begin{aligned} s_k \left(\theta_{i+1}^{(k)}, \theta_{i+1}^{(k+1)} \mid \theta_i^{(1)}, \theta_i^{(2)} \right) &= e^{(\beta_{k+1} - \beta_k) [U(\theta_{i+1}^{(k)}) + U(\theta_i^{(k)}) - U(\theta_{i+1}^{(k+1)}) - U(\theta_i^{(k+1)})]} \\ &\geq e^{(\beta_{k+1} - \beta_k)(2L - 2l)}. \end{aligned}$$

Denote by

$$\epsilon_0 := \min_{k=1, \dots, K-1} \left\{ \exp\{(\beta_{k+1} - \beta_k)(2L - 2l)\} \right\}. \quad (34)$$

Then, for any $k = 1, \dots, K-1$, we can get that, $1 \geq s_k \geq \epsilon_0 > 0$. For brevity, we take three chains as an example.

Proof of Theorem 5.5. By using Equation (34) and Lemma E.1, we obtain

$$\begin{aligned}
 & q\left(\theta' \mid \theta_i^{(1)}\right) \\
 &= \sum_{\theta_i^{(2)}} \sum_{\theta_{i+1}^{(2)}} \pi_{\alpha}^{\beta_2}\left(\theta_i^{(2)}\right) q_2\left(\theta_{i+1}^{(2)} \mid \theta_i^{(2)}\right)\left[1-s_1\left(\theta', \theta_{i+1}^{(2)}\right)\right] q_1\left(\theta' \mid \theta_i^{(1)}\right) \\
 &+ \sum_{\theta_i^{(3)}} \sum_{\theta_{i+1}^{(3)}} \sum_{\theta_i^{(2)}} \sum_{\theta_{i+1}^{(1)}} \pi_{\alpha}^{\beta_2}\left(\theta_i^{(2)}\right) q_2\left(\theta' \mid \theta_i^{(2)}\right) s_1\left(\theta_{i+1}^{(1)}, \theta'\right) q_1\left(\theta_{i+1}^{(1)} \mid \theta_i^{(1)}\right)\left(1-s_2\left(\theta', \theta_{i+1}^{(3)}\right)\right) q_3\left(\theta_{i+1}^{(3)} \mid \theta_i^{(3)}\right) \pi_{\alpha}^{\beta_3}\left(\theta_i^{(3)}\right) \\
 &+ \sum_{\theta_i^{(3)}} \sum_{\theta_i^{(2)}} \sum_{\theta_{i+1}^{(2)}} \sum_{\theta_{i+1}^{(1)}} \pi_{\alpha}^{\beta_2}\left(\theta_i^{(2)}\right) q_2\left(\theta_{i+1}^{(2)} \mid \theta_i^{(2)}\right) s_1\left(\theta_{i+1}^{(1)}, \theta'\right) q_1\left(\theta_{i+1}^{(1)} \mid \theta_i^{(1)}\right) s_2\left(\theta_{i+1}^{(2)}, \theta'\right) q_3\left(\theta' \mid \theta_i^{(3)}\right) \pi_{\alpha}^{\beta_3}\left(\theta_i^{(3)}\right) \\
 &\geq \epsilon_0^2 \sum_{\theta_i^{(3)}} \sum_{\theta_i^{(2)}} \sum_{\theta_{i+1}^{(2)}} \sum_{\theta_{i+1}^{(1)}} \pi_{\alpha}^{\beta_2}\left(\theta_i^{(2)}\right) q_2\left(\theta_{i+1}^{(2)} \mid \theta_i^{(2)}\right) q_1\left(\theta_{i+1}^{(1)} \mid \theta_i^{(1)}\right) q_3\left(\theta' \mid \theta_i^{(3)}\right) \pi_{\alpha}^{\beta_3}\left(\theta_i^{(3)}\right) \\
 &\geq \epsilon_0^2\left(\epsilon_{\beta_3, \alpha} \frac{\exp\left\{\beta_3 U\left(\theta'\right)\right\}}{\sum_{\theta' \in \Theta} \exp\left\{\beta_3 U\left(\theta'\right)\right\}}\right) \sum_{\theta_i^{(3)}} \sum_{\theta_i^{(2)}} \sum_{\theta_{i+1}^{(2)}} \sum_{\theta_{i+1}^{(1)}} \pi_{\alpha}^{\beta_2}\left(\theta_i^{(2)}\right) q_2\left(\theta_{i+1}^{(2)} \mid \theta_i^{(2)}\right) q_1\left(\theta_{i+1}^{(1)} \mid \theta_i^{(1)}\right) \pi_{\alpha}^{\beta_3}\left(\theta_i^{(3)}\right) \\
 &= \epsilon_0^2 \epsilon_{\beta_3, \alpha} \frac{\exp\left\{\beta_3 U\left(\theta'\right)\right\}}{\sum_{\theta' \in \Theta} \exp\left\{\beta_3 U\left(\theta'\right)\right\}}.
 \end{aligned}$$

□

Proof of Corollary 5.7. By using Theorem 5.5 and the fact $0 < \epsilon < 1$, we note that as the ϵ approaches 1, the sampling algorithm converges faster in terms of total variance. Specifically, we consider

$$k := \frac{\epsilon_0^2 \epsilon_{\beta_3, \alpha}}{\epsilon_{\beta_1, \alpha}} = \frac{\epsilon_0^2 \exp\left\{-\beta_3\left(\left(M-\frac{m}{2}\right) \tilde{\mathcal{D}}(\Theta)^2 - \|\nabla U(a)\| \tilde{\mathcal{D}}(\Theta)\right) - \frac{1}{\alpha} \tilde{\mathcal{D}}(\Theta)^p\right\}}{\exp\left\{-\beta_1\left(\left(M-\frac{m}{2}\right) \tilde{\mathcal{D}}(\Theta)^2 - \|\nabla U(a)\| \tilde{\mathcal{D}}(\Theta)\right) - \frac{1}{\alpha} \tilde{\mathcal{D}}(\Theta)^p\right\}}.$$

The multi-chain algorithm converges faster than single chain if $k > 1$. By using the definition of $\tilde{\mathcal{D}}$ and $\|\nabla U(a)\| < \left(M - \frac{m}{2}\right) \tilde{\mathcal{D}}(\Theta) - \frac{2 \log(1/\epsilon_0)}{\|\mathcal{T}_K\| \tilde{\mathcal{D}}(\Theta)}$ and the fact that $\beta_3 < \beta_1$, we obtain

$$\begin{aligned}
 k &= \epsilon_0^2 \exp\left\{(-\beta_3 + \beta_1)\left(\left(M-\frac{m}{2}\right) \tilde{\mathcal{D}}(\Theta)^2 - \|\nabla U(a)\| \tilde{\mathcal{D}}(\Theta)\right)\right\} \\
 &> 1
 \end{aligned}$$

Thus, we could conclude that the replica exchange algorithm converges faster than single chain langevin-like sampler in terms of Total Variance.

□

F. Additional Experiments Results and Setting Details

This section complements the main text by providing details on additional experimental procedures.

F.1. Sampling from Synthetic Energies

Synthetic Distribution We examine energy functions with varying components of Mixture of Gaussian Distributions (MoG) and Mixture of Student's t-Distributions (MoS) (Blessing et al., 2024), and use MMD and EMC to evaluate the algorithms' capability to navigate through complex terrains with multiple local minima and discontinuities.

The probability density function of **MoG** is given by:

$$p_{\text{MoG}}(\mathbf{x}) = \sum_{k=1}^{K_1} \pi_k \cdot \mathcal{N}(\mathbf{x} \mid \boldsymbol{\mu}_k, \boldsymbol{\Sigma}_k),$$

where K_1 denotes the number of Gaussian components, π_k denotes the mixing weight of the k -th component satisfying $\sum_{k=1}^{K_1} \pi_k = 1$ and $\pi_k > 0$, and $\mathcal{N}(\mathbf{x} \mid \boldsymbol{\mu}_k, \boldsymbol{\Sigma}_k)$ denotes the probability density function of a d -dimensional Gaussian distribution.

Similarly, the probability density function of **MoS** is given by:

$$p_{\text{MoS}}(\mathbf{x}) = \sum_{j=1}^{K_2} \pi_j \cdot t(\mathbf{x} \mid \boldsymbol{\mu}_j, \boldsymbol{\Sigma}_j, \nu_j),$$

where K_2 denotes the number of Student's t components, π_j denotes the mixing weight of the j -th component satisfying $\sum_{j=1}^{K_2} \pi_j = 1$ and $\pi_j > 0$, and $t(\mathbf{x} \mid \boldsymbol{\mu}_j, \boldsymbol{\Sigma}_j, \nu_j)$ denotes the probability density function of a d -dimensional Student's t -distribution.

EMC is the expected entropy of the auxiliary distribution, that is,

$$\text{EMC} := \mathbb{E}^{q_\theta} \mathcal{H}(p(\xi \mid \mathbf{x})) \approx -\frac{1}{N} \sum_{\mathbf{x} \sim q_\theta} \sum_{i=1}^M p(\xi_i \mid \mathbf{x}) \log_M p(\xi_i \mid \mathbf{x}),$$

where N denotes the number of samples drawn from q_θ .

MMD is a kernel-based test used to compare distributions which is computed as:

$$\text{MMD}^2(\pi, \tilde{\pi}) = \mathbb{E}_{\mathbf{x}, \mathbf{x}' \sim \pi} [k(\mathbf{x}, \mathbf{x}')] + \mathbb{E}_{\mathbf{y}, \mathbf{y}' \sim \tilde{\pi}} [k(\mathbf{y}, \mathbf{y}')] - 2\mathbb{E}_{\mathbf{x} \sim \pi, \mathbf{y} \sim \tilde{\pi}} [k(\mathbf{x}, \mathbf{y})],$$

where $k(\mathbf{x}, \mathbf{y})$ is a positive-definite kernel function. MMD measures the similarity between the empirical distributions of the generated and target samples. In practice, however, directly computing MMD is computationally expensive. Therefore, we use an approximation based on Random Fourier Features (RFF). The feature mapping is defined as:

$$\phi(X) = \sqrt{\frac{2}{D}} \cos(WX^\top + \mathbf{b}),$$

where $W \in \mathbb{R}^{D \times d}$ are random Gaussian variables sampled from $\mathcal{N}(0, 1/\sigma^2)$, and \mathbf{b} are random uniform variables in the range $[0, 2\pi]$. The parameter σ controls the kernel bandwidth, and D is the number of random features. For two distributions π and $\tilde{\pi}$, the empirical mean feature embeddings for $X \sim \pi$ and $Y \sim \tilde{\pi}$ are computed for both distributions:

$$\boldsymbol{\mu}_X = \frac{1}{n} \sum_{i=1}^n \phi(X_i), \quad \boldsymbol{\mu}_Y = \frac{1}{m} \sum_{i=1}^m \phi(Y_i).$$

The following approach allows us to efficiently compute the MMD between two distributions using RFF:

$$\text{MMD}^2(\pi, \tilde{\pi}) \approx \|\boldsymbol{\mu}_X - \boldsymbol{\mu}_Y\|^2.$$

KL divergence measures the difference between two probability distributions. Given the distributions π and $\tilde{\pi}$, the KL divergence is defined as:

$$D_{\text{KL}}(\pi \parallel \tilde{\pi}) = \sum_{\theta \in \Theta} \pi(\theta) \log \left(\frac{\pi(\theta)}{\tilde{\pi}(\theta)} \right),$$

where $\pi(\theta)$ represents the probability of θ under the target distribution π , and $\tilde{\pi}(\theta)$ represents the probability of θ under the empirical distribution $\tilde{\pi}$ obtained from sampling. This metric quantifies the information loss incurred when approximating the target distribution π using the empirical distribution $\tilde{\pi}$. A lower value of the KL divergence indicates better performance in approximating the target distribution.

Sampler Configuration DMALA is implemented with a step size of 0.15. For AB, the parameters are set to $\sigma = 0.1$ and $\alpha = 0.5$. ACS employs a cyclical step size scheduler with an initial step size of 0.6 over 10 cycles. For PTDL, we set the step size to 0.2 for all chains.

Table 4. MMD (\downarrow) results (MoG) across different components (c denotes the number of components)

Task	DMALA	ACS	AB	PTDLP
c=2	2.024 \pm 0.026	1.981 \pm 0.021	2.009 \pm 0.039	1.929 \pm0.027
c=4	2.042 \pm 0.023	1.994 \pm 0.016	1.992 \pm 0.012	1.924 \pm0.032
c=6	2.016 \pm 0.025	1.984 \pm 0.013	2.001 \pm 0.013	1.981 \pm0.025
c=8	2.077 \pm 0.022	2.004 \pm 0.011	2.019 \pm 0.036	1.996 \pm0.025
c=10	2.021 \pm 0.023	1.999 \pm 0.008	2.001 \pm 0.011	1.992 \pm0.009
c=12	2.089 \pm 0.043	2.033 \pm 0.039	2.024 \pm 0.012	2.002 \pm0.022
c=14	2.048 \pm 0.009	1.984 \pm 0.010	1.968 \pm 0.007	1.915 \pm0.024
c=16	2.030 \pm 0.012	2.006 \pm 0.013	2.001 \pm 0.012	1.924 \pm0.011

Table 5. MMD (\downarrow) results(MoS) across different components (c denotes the number of components)

Task	DMALA	ACS	AB	PTDLP
c=2	2.018 \pm 0.034	1.996 \pm 0.016	1.996 \pm 0.033	1.893 \pm0.029
c=4	2.109 \pm 0.012	1.997 \pm 0.009	1.994 \pm 0.007	1.957 \pm0.022
c=6	2.019 \pm 0.011	2.001 \pm 0.021	2.003 \pm 0.041	1.963 \pm0.019
c=8	2.017 \pm 0.021	2.006 \pm 0.017	2.005 \pm 0.024	1.934 \pm0.038
c=10	2.030 \pm 0.016	2.009 \pm 0.021	2.008 \pm 0.028	1.989 \pm0.012
c=12	2.014 \pm 0.024	1.994 \pm 0.030	2.001 \pm 0.017	1.964 \pm0.023
c=14	2.095 \pm 0.019	2.001 \pm 0.022	2.003 \pm 0.028	1.944 \pm0.016
c=16	2.158 \pm 0.023	2.013 \pm 0.021	2.015 \pm 0.018	1.967 \pm0.015

Results When the number of components in both MoG and MoS varies, our sampler consistently achieves significantly superior MMD and EMC scores compared to DMALA, ACS, and AB. Its capacity to effectively distribute samples, even in scenarios characterized by disconnected modes and steep energy barriers, underscores its robustness in navigating intricate discrete energy landscapes.

F.2. RBM Sampling

RBM introduction We will give a brief introduction of the Block-Gibbs sampler used to represent the ground truth of the RBM distribution. For a more in-depth explanation, see [Grathwohl et al. \(2021\)](#). Given the hidden units h and the sample θ , we define the RBM distribution as follows:

$$\log p(\theta, h) = h^\top W \theta + b^\top \theta + c^\top - \log Z$$

As before, Z is the normalizing constant for the distribution. The sample x is represented by the visible layer with units corresponding to the sample space dimension and h represents the model capacity. It can be shown that the marginal distributions are as follows:

$$p(x | h) = \text{Bernoulli}(Wx + c)$$

$$p(h | x) = \text{Bernoulli}(W^\top h + b)$$

The Block-Gibbs sampler updates θ and h alternatively, allowing for many of the coordinates to get changed at the same time, due to utilizing the specific structure of the RBM model.

Experiment Setup We follow the experimental setup of [Zhang et al. \(2022\)](#) and use RBM models with 500 hidden units and 784 visible units. We adopt the same training protocol, except we train the RBM with 100 steps of Contrastive Divergence as opposed to 10. We train the models for one pass through the dataset.

Sampler Configuration For DMALA, we set step size to 0.2, and for AB we use the default hyper-parameters for the first order sampler. For ACS, we use $\rho^* = 0.5$, $\beta_{\max} = 0.95$, $\zeta = 0.5$, cycle length $s = 20$ for all the datasets. We also fix the total overhead of the tuning algorithm to 10% of the total sampling steps. For PTDLP, we set the step size to 0.15 \sim 0.45 for all chains.

Escape from Local Modes In addition to using the same initialization as Grathwohl et al. (2021); Zhang et al. (2022), we extend the experiment to measure the ability of a sampler to escape from local modes. We initialize the sampler within the most likely mode, as measured by unnormalized energy of the RBM. Samplers that are less prone to getting trapped in local modes will be able to converge quicker to the ground truth, as measured by log MMD. We include the performance of the various samplers across 5 random seeds in Figure 3. PTDL P demonstrates superior robustness to mode-specific initialization due to its capability to escape from local modes.

Generated Images We found that a visual inspection of the generated images demonstrates the ability of PTDL P to escape local modes. We include the generated images in Figure 4.

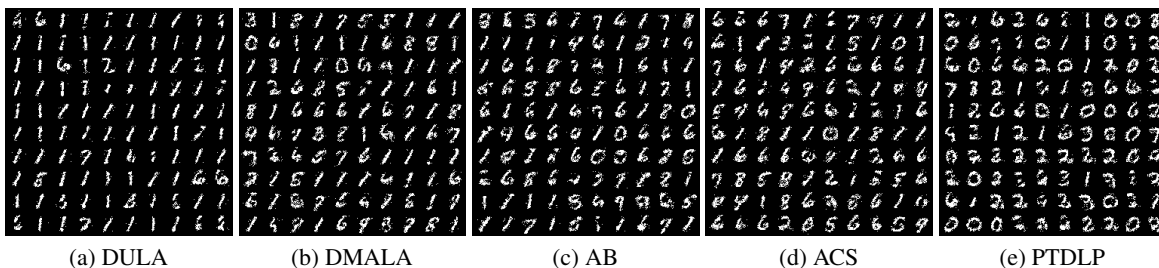


Figure 4. Images sampled from RBM trained on MNIST when the sampler is initialized to most likely mode. Our algorithm is able to generate a diverse range of digits, demonstrating its ability to escape from modes.

F.3. RBM Learning

Experiment Design We use the same RBM structure as the sampling task, with 500 hidden units and 784 visible units. We apply the samplers of interest to the PCD algorithm introduced by Tieleman (2008). The model parameters are tuned via the Adam optimizer with a learning rate of .001.

Sampler Configuration For DMALA, we set step size to 0.2, and for AB we use the default hyper-parameters for the first order sampler. For ACS, we follow the setting in Pynadath et al. (2024) and use $\rho^* = 0.5, \beta_{\max} = 0.95, \zeta = 0.5$, cycle length $s = 20$ for all the datasets. We also fix the total overhead of the tuning algorithm to 10% of the total sampling steps.

F.4. Learning EBMs

Experiment Setup We adopt the same ResNet structure and experiment protocol as in Grathwohl et al. (2021), where the network has 8 residual blocks with 64 feature maps. There are 2 convolutional layers for each residual block. The network uses Swish activation function (Ramachandran et al., 2017). For static/dynamic MNIST and Omniglot, we use a replay buffer with 10,000 samples. For Caltech, we use a replay buffer with 1,000 samples. We evaluate the models every 5,000 iterations by running AIS for 10,000 steps. The reported results are from the model which performs the best on the validation set. The final reported numbers are generated by running 300,000 iterations of AIS. All the models are trained with Adam (Kingma, 2014) with a learning rate of 0.001 for 50,000 iterations.

Sampler Configuration For DMALA, we use a step size of 0.15 as used in Zhang et al. (2022). For ACS, we follow the setting in Pynadath et al. (2024) and use 200 sampling steps for EstimateAlphaMax and EstimateAlphaMin. For Static MNIST, Dynamic MNIST, and Omniglot, we set the algorithm to tune α_{\max} and α_{\min} every 25 cycles, where each cycle has 50 training iterations. For Caltech Silhouettes, we have to adapt every 10 cycles with the same number of training iterations. We set the step sizes as $0.05 \sim 0.4$ for all chains in our algorithm.

Generated Images Here we provide the generated results in Figure 5 from our algorithm across Static MNIST, Dynamic MNIST, Omniglot, and Caltech Silhouettes. These images demonstrate the ability of trained deep EBMs to capture the underlying data distribution. The deep EBM is capable of producing high-quality samples that visually resemble the training data, which indicates that the learned energy function effectively models the complex, high-dimensional structure of the data.

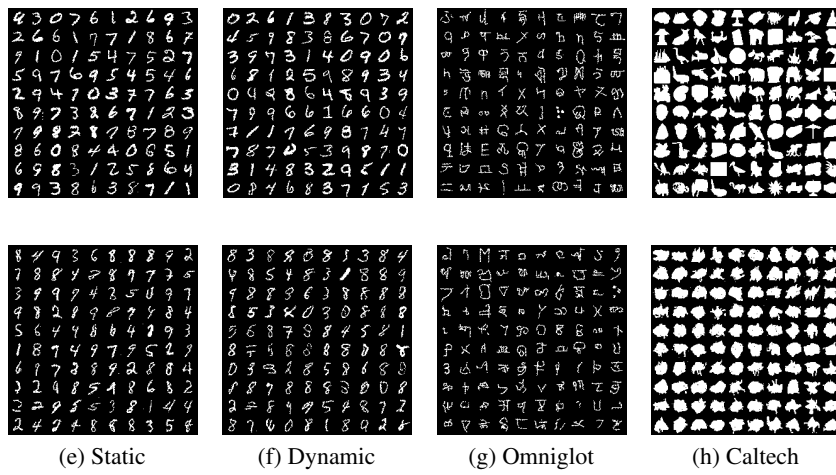


Figure 5. The images on the top row are examples from the dataset, while the bottom row are from the trained EBM. The images generated from our algorithm are similar to those from the dataset, demonstrating that the model is capable of generating high-quality samples.